Aus dem Institut für Radiologie

der Medizinischen Fakultät Charité – Universitätsmedizin Berlin

DISSERTATION

Linking Prostate Cancer Recurrence to the Spermine Pathway: A Retrospective Study using High Resolution Magic Angle Spinning ^{1}H Magnetic Resonance Spectroscopy at 14T and Quantitative Polymerase Chain Reaction

zur Erlangung des akademischen Grades
Doctor medicinae (Dr. med.)

vorgelegt der Medizinischen Fakultät
Charité – Universitätsmedizin Berlin

von
Florian Paul Sturm
aus Tettnang

Gutachter/in:

1. Prof. Dr. med. M. Taupitz
2. Prof. Dr. med. V. Nicolas
3. Priv.-Doz. Dr. med. C. Kempkensteffen

Datum der Promotion: 30.11.2012

Acknowledgments

I am grateful to Dr. Leo L. Cheng, Assistant Professor of Radiology and Pathology, Massachusetts General Hospital, Harvard Medical School, for his continuous encouragement and mentorship and for making this research project possible. I am equally grateful to Prof. Dr. med. Matthias Taupitz, Institut für Radiologie, Medizinische Fakultät Charité – Universitätsmedizin Berlin, for his invaluable guidance and support.

Table of Contents

1 Introduction and background 6

1.1 Prostate cancer, PSA and biochemical recurrence 6
1.2 Prostate cancer diagnostics 8
1.2.1 The current state of prostate cancer diagnostics 8
1.2.2 Current challenges in prostate cancer diagnostics 9
1.2.3 The diagnostic potential of HRMAS ^{1}H MRS 10
1.2.4 Results from a preceding study 12
1.3 Prostate cancer and spermine 14
1.3.1 The inhibitory function of spermine 14
1.3.2 The polyamine pathway 16
1.4 Hypotheses tested by the study 18
1.4.1 Primary hypothesis 19
1.4.2 Secondary hypothesis 20

2 Materials and methods 21

2.1 Study design and patient population 21
2.2 Histopathological assessment 25
2.3 Quantitative methods 27
2.3.1 HRMAS ^{1}H MRS 27
2.3.2 QPCR 28
2.4 Data processing 36
2.4.1 HRMAS ^{1}H MRS 36
2.4.2 QPCR 37
2.5 Statistical analysis 41
2.5.1 General note on statistical significance 41
2.5.2 Specific statistical parameters 41
2.6 Contributions by the author 43

3 Results 45

3.1 Preliminary methodological findings 45
3.1.1 Proof of concept of qPCR 45
3.1.2 Congruence of quantification methods for qPCR 46
3.2 Primary hypothesis 48
3.2.1 Individual enzymes 48
3.2.2 Combined model 51

3.3 Secondary hypothesis 52
3.3.1 Individual enzymes 52
3.3.2 Combined model 55
3.4 Additional findings 57
3.4.1 c-Myc 57
3.4.2 Correlation of anabolic enzymes 57
3.4.3 Correlation of catabolic enzymes 58
3.4.4 Inverse correlation of SSAT and Anabolic Enzymes 59

4 Discussion 61
4.1 Preliminary methodological findings 61
4.2 Principal findings 61
4.3 Principal findings in the context of current literature 64
4.4 Principal findings and clinical application 65
4.5 Limitations 69
4.5.1 Study design 69
4.5.2 Methods 70
4.6 A research agenda 71
4.6.1 Study design 71
4.6.2 Methods 72

5 Summary 74

Zusammenfassung 76

List of Abbreviations 77
List of Figures 79
List of Tables 82
Bibliography 84

Selbstständigkeitserklärung 98
Curriculum Vitae ..... Fehler! Textmarke nicht definiert.

1 Introduction and background

1.1 Prostate cancer, PSA and biochemical recurrence

Prostate cancer (PCa) is the most frequently diagnosed malignancy in adult males (1). In Germany, PCa ranks third as a cause of cancer death in men, trailing only lung and colorectal cancer (2). For the United States of America, PCa is the second leading cause of cancer death in men, being outranked by lung cancer only (1). In the US, 83 men die of the disease every day (3, 4).

Both the prevalence of and mortality from the disease have increased steadily in the last two decades, due partly to shifting and improving diagnostic paradigms and partly to demographic changes (5). Epidemiologically, age is a prime risk factor for the development of PCa. The average age at the time of diagnosis is 70 (6).

The biological behavior of PCa is special among solid tumors in that it is characterized by a comparatively slow and prolonged evolution from the diagnosis of localized disease to metastatic disease progression to prostate cancer specific-mortality (7, 8). After undergoing prostatectomy, very few patients will die from the disease or its effects, such as metastases, within the initial 15 years after the procedure (7). This may be due to either the low lethality of PCa detected in screenings or the effectiveness of radical prostatectomy, or both (9).

The diagnostics of the disease has made a major leap forward with the introduction of serum prostate-specific antigen (PSA). Besides its prime function as a screening parameter for the detection of PCa, it also serves as monitoring parameter after radical prostatectomy. PSA is routinely used to track disease recurrence after surgical removal of the prostate, based on the established finding that an elevation of PSA typically precedes metastatic progression and prostate-specific mortality by an average of 7 to 15 years, as metastases begin to produce the metabolite again (10, 11). Metastatic progression in turn antedates prostate-specific mortality by an average of 3 to 6 years (9, 10, 12).

This detection of PSA after radical prostatectomy has been labeled ‘biochemical recurrence’ (BCR). Alternative terminologies include ‘PSA failure’, ‘chemical failure’ and ‘biochemical relapse’ (8). The absence of BCR is diagnostically valuable as it serves as an early endpoint of treatment success. The detection of BCR, on the other hand, may herald the metastatic progres-

sion of the disease. BCR is also crucial on the therapeutic level as it may prompt clinicians to initiate further therapy during an otherwise largely asymptomatic phase of the disease.

It is important to note that the progression of prostatic disease after BCR may vary significantly. Although BCR ultimately foreshadows distant metastasis and prostate-specific mortality, the speed and severity of the progression diverge considerably between different cases (13). During the first 15 years after the first detection of BCR, patients are, on average, as likely to die from prostate cancer as they are from competing causes (14). A slow or moderate PSA rise may change neither the patient's expected length of life nor his expected quality of life (15). The development of diagnostic markers to distinguish between more and less aggressive cases of BCR is therefore crucial.

Although PSA is a commonly accepted screening instrument both pre and post prostatectomy, its exact definition has been the subject of considerable debate and definitions across different scientific publications vary greatly (8). This is especially dramatic as the definition of BCR may in turn have weighty effects on outcome reporting and may hence distort treatment evaluations. Estimates of disease progression rates vary by up to 35% between different definitions of BCR (16-18). If, for example, BCR is defined as the transgression of a 0.2 versus a 0.4 ng/ml PSA threshold, the likelihood of secondary therapy and the likelihood of PSA progression ranged from 50% to 79% (18). In another study, the 10-year progression probability varied from 63% to 79% (8).

Clearly, a standardized definition is essential. It facilitates comparisons between local therapies or combined modality treatment strategies, it facilitates the identification of patients most suited for entry into clinical trials and it facilitates the selection of patients for salvage therapy (19).

Most crucially, any common definition of BCR will exhibit close correlation with the primary endpoints of metastatic progression and prostate-specific mortality. Stephenson et al. examined 10 common definitions of BCR for these features. A definition of BCR as a PSA of at least 0.4 ng/ml followed by another increase had the highest calculated R^2 statistic with metastatic progression when controlled for secondary therapy and other prognostic parameters (8). Based on this definition, the 15-year likelihood of prostate-cancer specific mortality following biochemical recurrence is 12%, as compared to a 38% all-cause mortality (7).

The definition of BCR that the original sample selection in this study was based on (initial PSA >0.2 ng/ml, followed by another increase) exhibited a slightly lower, but also justifiably close R^2 correlation with the primary endpoints of metastatic progression and prostate cancer-specific mortality (8). Details of the PSA scores of the individual samples are listed in the methods section.

1.2 Prostate cancer diagnostics

1.2.1 The current state of prostate cancer diagnostics

A variety of clinical tools are available for PCa diagnostics. Transrectal ultrasound is the most commonly applied method in symptomatic patients. Less frequently used are magnetic resonance imaging and magnetic resonance spectroscopy (20). Patients are typically selected for these diagnostic procedures following abnormal results in routine diagnostics, such as an abnormal digital rectal examination or an elevated serum PSA. Less frequently, patients will be selected for further diagnostics based on symptomatic clinical events, such as pollakisuria, dysuria, hematuria, difficulty starting and maintaining a steady stream of urine or erectile dysfunction (20). Following these first stage diagnostic tools, critical cases are submitted for a transrectal, ultrasound-guided needle biopsy.

Biopsies are taken by a biopsy gun, with now twelve tissue cores as the standard number of site samples (20, 21). The tissue specimens obtained are then histopathologically evaluated. In sum, PSA test plus biopsy thus constitute the standard diagnostic protocol for local PCa (22, 23).

Histopathological assessment of the specimens typically follows the Gleason Score (GS) scheme (24-29). Under this scheme, values between 2 and 10 are assigned to each specimen. The score represents the sum of two subordinate scores: one score for the dominant primary tumor growth pattern found in the specimen (values of 1 to 5) and one for the sub-dominant secondary growth pattern (values of 1 to 5). GS ratings of 2 to 4 are labelled ‘well-differentiated disease’, ratings of 5 to 7 ‘moderately differentiated adenocarcinomas’ and ratings of 8 to 10 ‘poorly differentiated cancers’ (30).

Positive PCa biopsy results are then used in a battery of nomograms to determine the likelihood of extracapsular extension and seminal vesicle invasion as well as lymph node metastases (31,

32). Higher Gleason Scores are generally associated with a higher likelihood of extracapsular spread, nodal involvement, and metastases (33).

After prostatectomy, histopathological assessment can be paired with clinical findings to stage the carcinoma according to the American Joint Commission on Cancer (AJCC) system, which includes the characteristics of the original tumor, lymph node spread and metastases (TNM).

Based on pre-prostatectomy histopathological findings only, however, 70% of cancers diagnosed after PSA elevation are GS 6 and 7 tumors, i.e. moderately differentiated adenocarcinomas (20, 30, 34). For this subgroup, no reliable further differentiation in terms of tumor aggressiveness and probability of clinically significant progression is currently available pre-prostatectomy.

Serum PSA tests are used as the standard follow-up instrument after prostatectomy. PSA tests here serve a joint purpose: Firstly, monitoring therapy response; secondly, detecting BCR (35).

1.2.2 Current challenges in prostate cancer diagnostics

One chief focus of research in the area of PCa is the search for new diagnostic markers. Another focus is the clarification of basic disease mechanisms, often coupled with the intention of therapy design (36-38). In many cases, both objectives are simultaneously tackled (39-50).

On the diagnostic side, three specific objectives are part of the research agenda: Firstly, an improved prognostic discrimination among moderately differentiated adenocarcinomas. The introduction of PSA testing led to a rising incidence of early stage PCa diagnoses. While this offers the opportunity of timely therapeutic intervention, it is not always clear whether intervention or which intervention is the best clinical choice. This is especially noteworthy as the main therapeutic choice, radical prostatectomy, may have serious and irreversible consequences for the individual patient. Every day, of the on average more than 150 patients undergoing radical prostatectomy in the US, more than 45 will be permanently incontinent and more than 90 permanently impotent (51).

Currently, using the best available empirical nomograms, aggressive and indolent cancer types can be distinguished with a maximum certainty of only 80% and less (52-56). For the subgroup of moderately differentiated GS 6 and GS 7 types, i.e. the vast majority of PCa patients, the op-

timal courses of treatment are difficult to determine. Clinical evidence consequently suggests that treatment outcomes for this subgroup vary greatly (10, 20, 34). The prevalent scientific opinion suggests that differences in biological tumor aggressiveness are the root cause of this variation. Developing diagnostic tools quantifying these biological differences is therefore one of the main challenges in current PCa diagnostics (57, 58).

A second objective of the PCa research agenda is a better diagnostic exploitation of rising PSA levels. PSA may be elevated due to a number of reasons. Two of the more frequent ones are prostatitis and benign prostatic hyperplasia (BPH) (59). Efforts to distinguish these benign conditions from PCa have, to present an example, led to the identification of P504S, a protein involved in beta-oxidation of fatty acids, as a more specific supplementary marker (60). Immunohistochemical staining for P504S has been shown to differentiate benign from malignant lesions, and an atypically proliferating early stage of PCa from benign lesions (61-64).

A third objective of the PCa research agenda is an improved prediction of BCR and, intimately linked to BCR, an improved prediction of metastatic progression of the disease. At best, a first probabilistic judgment of recurrence would be available at the time of prostatectomy already, to guide follow-up regimes. At present, PSA test results, GS and clinical staging are incorporated in empirical nomograms to assess the likelihood of BCR preoperatively (65-68). However, the postoperative use of these preoperative nomograms is limited: As TNM pathological information becomes available after prostatectomy, this new information routinely decides on the course of therapy (69, 70). One challenge is thus the improved pre- and postoperative prediction of BCR. The present study is aimed at making a contribution to specifically this objective.

1.2.3 The diagnostic potential of HRMAS ^{1}H MRS

Many of the challenges of current PCa diagnostics discussed above can potentially be addressed by magnetic resonance spectroscopy (MRS) in general and High Resolution Magic Angle Spinning Proton Magnetic Resonance Spectroscopy (HRMAS ^{1}H MRS) in particular.

MRS is a diagnostic method with an extremely high sensitivity for differences in biochemical tissue profiles. It can serve as a quantification method for metabolites and as a detection method for abnormal cells (71, 72). Demonstrating its sensitivity, MRS has, for example, been shown to detect microscopic metastatic deposits in lymph nodes that had gone undetected by histopathol-

ogy (73). As a general technical principle, MRS extracts its information by observing how nuclei behave in a magnetic field when a second perturbing oscillating magnetic field is added (74). While routine magnetic resonance imaging (MRI) scans yield anatomical information about a tumor, MRS is targeted at its biochemical features (75). It may be used to determine metabolite concentrations and to re-construct metabolomic profiles of the examined tissue.

Studies based on ^{1}H MRS have identified various potential clinical markers for PCa *in vivo* (76-88). *Ex vivo* studies have used a variety of materials, most commonly cell lines, but also prostate fluid, serum and other body fluids, and solutions of tissue extracts, to advance the diagnostic use of PCa markers (89-98).

Both approaches face various difficulties. Studies applying *in vivo* MRS methods cannot readily match MRS results with pathological information. Studies applying e*x vivo* MRS methods face a twofold dilemma: Firstly, they are based on the assumption that the differences between aqueous homogenous solutions and non-liquid tissue are negligible. Empirical studies have shown, however, that the process of extraction changes the metabolic features of the tissue significantly. Secondly, once extracted, the original material cannot be used for pathological examination any more (99).

The technical innovation of HRMAS ^{1}H MRS is the fact that it makes magnetic resonance spectroscopy of intact solid state tissue possible. Conventional MRS methods had previously only been applied to extracts and lysed cell solutions, as molecules are largely free from reciprocal effects in these media. When applied to solid structures, however, conventional MRS methods cause disintegration as molecules experience anisotropic effects. Technically, this disintegration causes spectral line broadening which in turn renders the distinction of individual metabolites impossible. Using conventional MRS methods, in consequence of the disintegration, tissue cannot subsequently be submitted for pathological evaluation.

HRMAS ^{1}H MRS overcomes these difficulties by spinning the tissue sample around a ‘magic angle’ axis vis-à-vis the direction of the magnetic field, namely a 54.7° angle between the 1/1/1-vector and the z-axis (100). At sufficiently high rates, the spinning averages anisotropic interaction to isotropic levels. The technical effect of this averaging is a line-narrowing that sufficiently increases spectral resolution to identify and quantify individual metabolites. At the same time, tissue structures are preserved and enable subsequent pathological examination and other quantitative methods (101).

The material used in HRMAS ^{1}H MRS is therefore a largely unaltered version of the original tissue and its biochemical state. Following its early development (102, 103), HRMAS ^{1}H MRS has found broad investigative application, both in PCa diagnostics and, among others, in studies of breast cancer, melanoma, liposarcoma, glioblastoma, kidney carcinoma and malignant lymph nodes (104-136). Note, however, that while ^{1}H MRS is in principle available both for *in vivo* and *ex vivo* studies, HRMAS ^{1}H MRS is at present only available for *ex vivo* application (81, 119, 137, 138).

The spectroscopy data of the present study were produced using HRMAS ^{1}H MRS exclusively. Using this method enabled us to match spectroscopy data with pathological data and data from quantitative methods of molecular biology. A detailed explication is given in the methods section.

1.2.4 Results from a preceding study

Recognizing its diagnostic potential, a preceding study applied HRMAS ^{1}H MRS to the task of predicting BCR of PCa (139). The study retrospectively matched 16 cases of known BCR with 16 non-recurrent cases. Individual cases were paired on the basis of age, Gleason score and clinical staging. *Ex vivo* intact 14T spectroscopy results of specimens (gained at the time of prostatectomy for the individual cases) were statistically analyzed, identifying 27 principal components of spectral regions. The most significant contributors to the overall metabolomic profile among these principal components were subsequently used to construct a canonical score. This canonical score effectively differentiated between recurrent and non-recurrent cases, based solely on MRS information about the individual cases. Testing the coefficients from the principal component analysis and the canonical score on a second group of non-recurrent cases (n=16, matched to the original BCR cases based on age, Gleason Score and pathological stage), a predictive accuracy of BCR of 78% was achieved (139). Figure 1 illustrates the principal finding of the study.

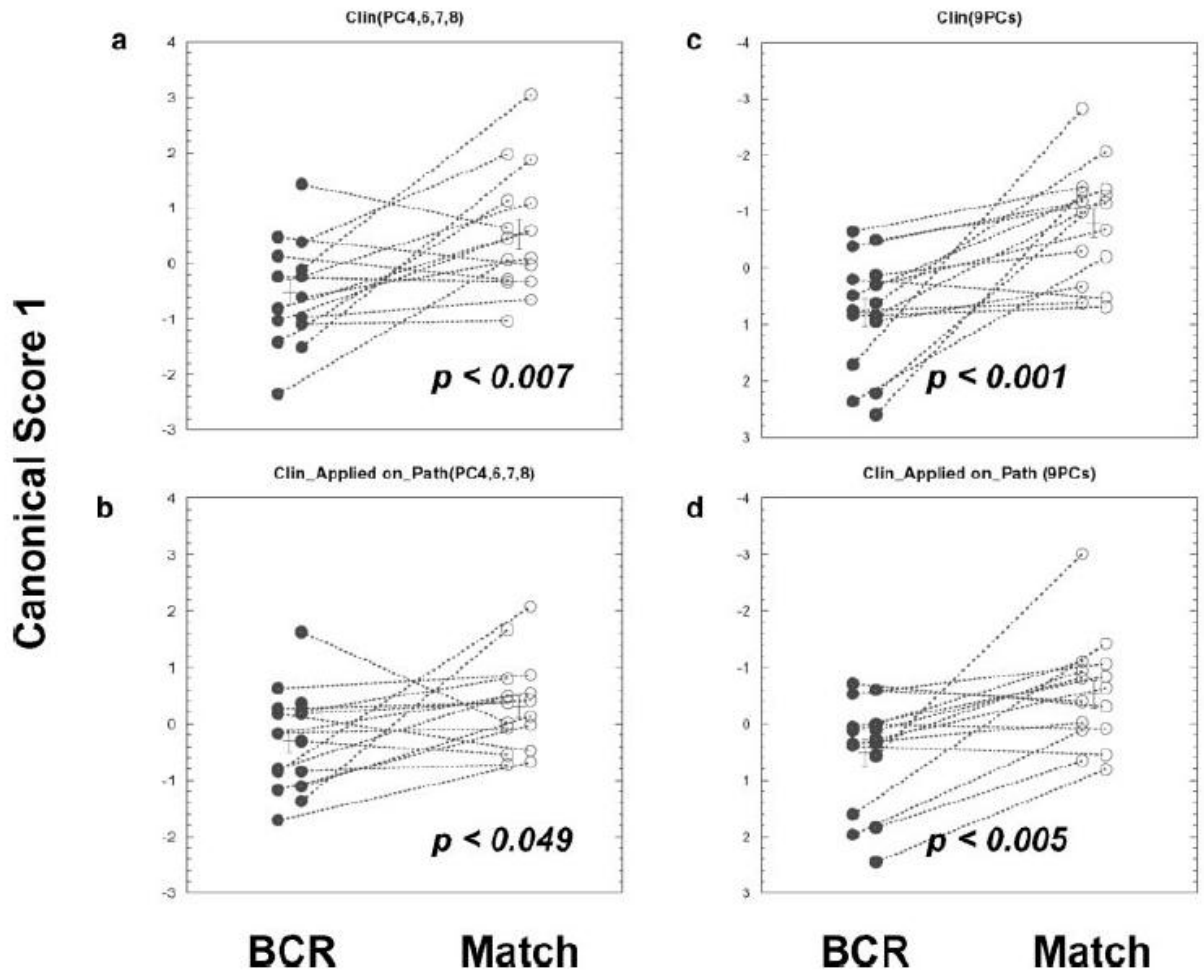

Figure 1 **Results from a preceding study.** The study identified 27 spectral regions, constructing a canonical score from selected principal components as the metabolomic profile of prostate cancer recurrence. The canonical score differentiates between cases of biochemical recurrence (BCR) and cases without recurrence of PCa (match) with statistical significance. The left two plots use the four and the right two plots the nine statistically most influential principal components. The upper two plots compare the recurrent group with a non-recurrent group matched by clinical staging. The lower two plots apply the score to a second non-recurrent group matched by pathological staging (139).

The present study follows up on the encouraging results of this preceding study, adding to MRS metabolomic profiles the enzymatic profiles established by methods of molecular biology. Detailed objectives of the present study and the specific hypotheses tested are discussed below. Details regarding the spectroscopy methods of the preceding study are discussed in the methods section.

1.3 Prostate cancer and spermine

1.3.1 The inhibitory function of spermine

Among a broad variety of substances hypothesized to have an inhibiting effect on PCa, the polyamine spermine plays a special and indeed intriguing part. For one, it is an endogenous metabolite, and would as such be part of the human body's own defense lsines against cancer. Secondly, it is abundantly found in the prostate – more abundantly, in fact, than in any other organ of the human body (140). This would correspond to the fact discussed above that prostate cancer has, when compared to other solid tumors, an extremely prolonged progression of disease.

Various studies have supported the view that spermine acts as an endogenous inhibitor of PCa. Initially, the relation was demonstrated via *in vitro* cell line studies. Aqueous extracts of human prostate tissue were found to block prostatic carcinoma proliferation *in vitro* (and subcutaneous tumor expansion in *vivo*). Purification and biochemical characterization disclosed spermine as the decisive inhibiting substance of the study (141).

In the wake of this discovery, numerous studies have dealt with the potential role of spermine in cancer diagnostics and cancer therapy (142-158). In a study using ^{1}H MRS to construct metabolic profiles (from expressed prostatic secretions) for 52 subjects with PCa, spermine, alongside citrate and myo-inositol, was found to be highly predictive of the disease and inversely related to the risk of PCa when compared to 26 healthy controls. The study calculated the area under the curve (AUC) of the receiver operating characteristic (ROC) curve for spermine to be 0.79 (159).

Studies combining MRS and high-pressure liquid chromatography (HPLC) also showed that normal and benign hyperplastic tissue exhibited a relatively high content of spermine when compared to PCa tissue. Particularly low levels of spermine were found in those cases of PCa that were associated with clinically detected metastases. Using the typical clinical field strength of 1.5 T, spermine *in vitro* signals were found to reside in the region between 3.0 and 3.3 ppm. In *in vivo* prostate MR spectra the spermine signals overlapped, however, with the resonances of creatine and choline at 3.0 ppm and 3.2 ppm, respectively, distorting the spermine-specific results (93).

Combining HRMAS ^{1}H MRS at 9.4 T (400 MHz) with quantitative histopathology, a further study demonstrated a linear correlation between NMR spermine concentrations and the volume percentage of benign epithelial cells in human prostate. Again, the usage of non-destructive

HRMAS ^{1}H MRS instead of conventional MRS made it possible to produce spectroscopy data and histopathological data from the same intact specimen (160). A typical spectrum produced by HRMAS ^{1}H MRS is depicted in Figure 2. Figure 3 reproduces the key chart of the study demonstrating the linear relationship between spermine concentration and percentage volume of benign epithelial tissue.

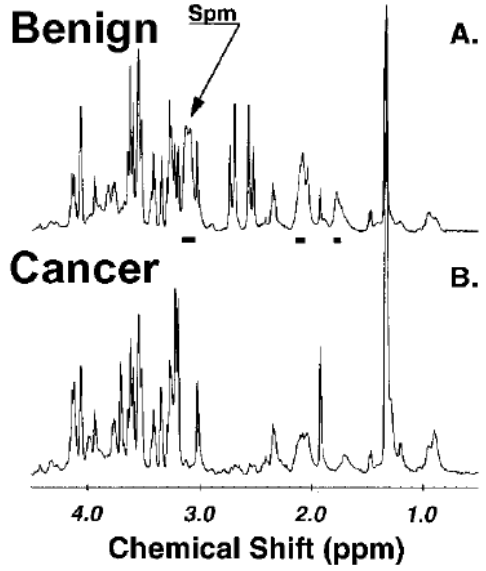

Figure 2 Magnetic resonance spectrum of benign and malignant prostate tissue. The spermine peak in the metabolomic profile differs between benign (A) and cancerous tissue (B). The spectra stem from HRMAS ^{1}H MRS at 9.4 T (400 MHz) (160).

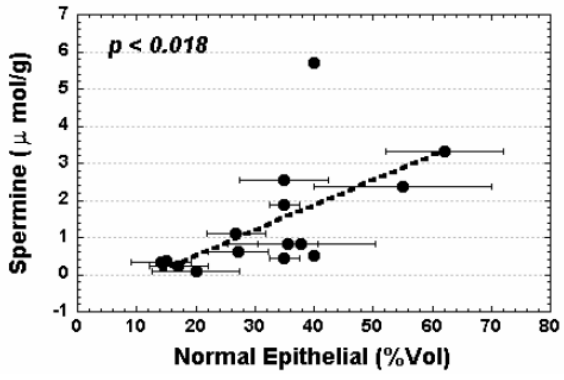

Figure 3 Correlation between spermine concentration and volume percentage of benign epithelium. The figure reproduces the key chart of the preceding study demonstrating that spermine concentrations as measured by MRS and volume percentage of benign epithelium as measured by quantitative histopathology correlate (160).

In sum, there is strong evidence that spermine serves as an endogenous inhibitor of PCa. Given this, the metabolic pathway regulating spermine levels in prostate tissue is of critical interest for PCa diagnostics and therapy.

1.3.2 The polyamine pathway

Together with putrescine and spermidine, spermine belongs to the polyamine molecule family. All members of the family are derived from ornithine via a process of decarboxylation and condensation. Spermine is the preliminary endpoint of this biochemical transformation, starting from ornithine and with putrescine and spermidine as intermediate steps in the process (161-163). The complete spermine pathway is illustrated in Figure 4.

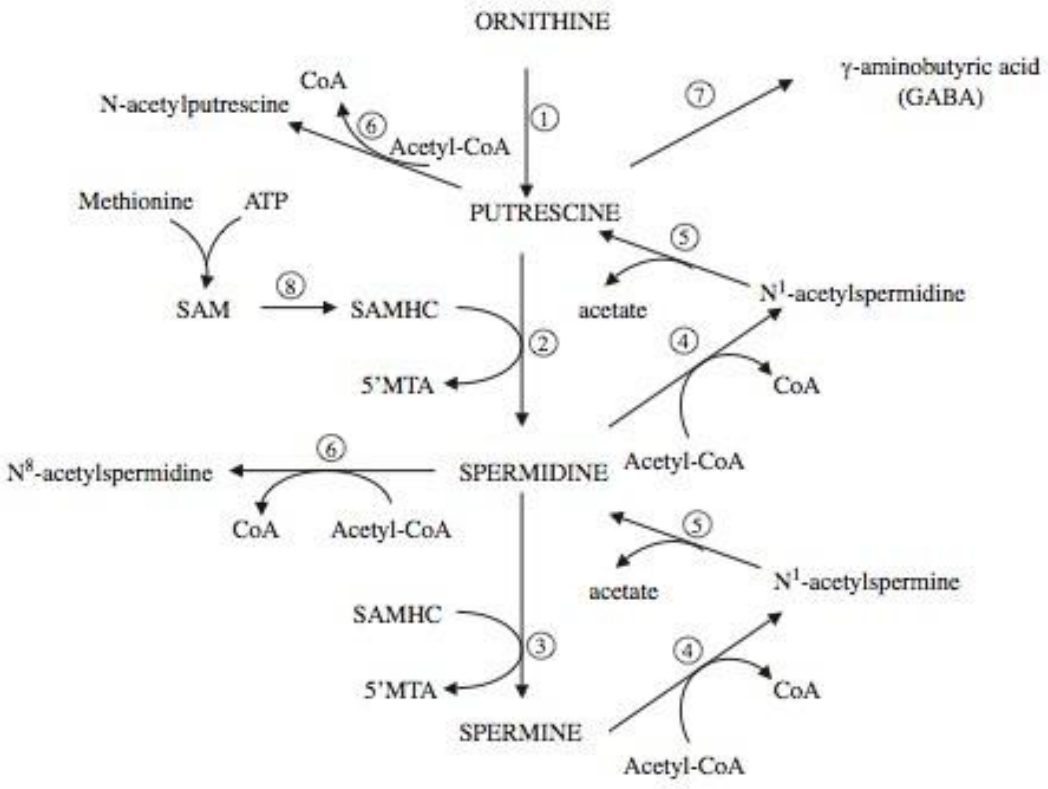

Figure 4 The polyamine pathway. Spermine is produced from ornithine in a sequence of steps with putrescine and spermidine as metabolic predecessors and a total of eight different enzymes directly catalyzing the process (161). Names of the enzymes 1 to 8 are given in Table 1. 5MTA: 5-methylthioadenosine; SAM: S-adenosyl-methionine; SAMHC: S-adenosyl-S-methyl homocysteamine.

The pathway is under complex enzymatic control. Ornithine decarboxylase (ODC) launches polyamine synthesis by producing putrescine, a diamine. Spermine is then created by the consecutive addition of two aminopropyl groups forming first spermidine, then spermine. Both aminopropyl groups ultimately stem from methionine via the decarboxylation of S-adenosyl-methionine, a step catalyzed by the S-adenosyl-methionine decarboxylase (AdoMetDC) (163).

Backward conversion from spermine to spermidine, and from spermidine to putrescine is catalyzed by the acetyl-CoA spermidine/spermine N1-acetyl-transferase (SSAT). It is the rate limiting catabolic enzyme of the pathway. The rate limiting anabolic enzymes are ODC and AdoMetDC (163).

ODC, as a major player of spermine synthesis, is regulated on a number of levels. One level is the enzymatic control by its antizyme, the ornithine decarboxylase antizyme (OAZ). Inhibition occurs through OAZ binding to ODC and through OAZ promoting the degradation of ODC. OAZ itself is auto-regulated by translational frameshifting stimulated by polyamine levels (164, 165). All enzymes involved in the spermine pathway are listed in Table 1.

Number	Enzyme	Short name
1	Ornithine decarboxylase	ODC
2	Spermidine synthetase	-
3	Spermine synthetase	-
4	Acetyl-CoA spermidine/spermine N1-acetyl-transferase	SSAT
5	Polyamine oxidase	PAO
6	N-acetyl transferase	-
7	Diamine oxidase	DAO
8	S-adenosyl-methionine decarboxylase	AdoMetDC
(1)	Ornithine decarboxylase antizyme	OAZ

Table 1 Enzymes of the polyamine pathway. Numbers refer to Figure 4. There are three rate-limiting enzymes involved in the pathway. Ornithine decarboxylase (ODC) and S-adenosyl-methionine decarboxylase (AdoMetDC) are the rate limiting anabolic enzymes, while acetyl-CoA spermidine/spermine N1-acetyl-transferase (SSAT) is the rate limiting catabolic enzyme.

The formal chemical makeup of spermine is $^{+}H_3N\text{-}(CH_2)_3\text{-}NH\text{-}(CH_2)_4\text{-}NH\text{-}(CH_2)_3\text{-}NH_3^{+}$. In addition to the enzymatic regulation described above, its total intracellular concentration is also influenced by exit into and entry from the extracellular compartment (166).

Although first detected in seminal fluid, polyamines are found in all normal human body cells and play a crucial role in cell growth, maintenance and function. PCa is only one of a variety of pathological processes where polyamine control appears to be dysfunctional. Various strategies of therapy and nutritional benefit are targeted at this family of molecules (161).

Regarding the pathological processes taking place in prostatic cancerous tissue, we found in a previous study that the mRNA expression levels of spermine anabolic enzymes logarithmically decrease as PSA velocity increases. In contrast, the mRNA expression level of OAZ, i.e. the antizyme of the rate limiting anabolic player, increased as PSA velocity increased. PSA velocity, in turn, has been extensively discussed as a marker for prostatic tumor aggressiveness. ODC and OAZ mRNA expression levels were found to correlate inversely (140).

1.4 Hypotheses tested by the study

The recurrence of PCa as heralded by rising PSA levels foreshadows the metastatic progression of the disease. And it is critically linked to PCa-specific mortality. Diagnostic tools of early detection of BCR and predictive tools estimating the likelihood of BCR would significantly improve therapeutic strategies and enable clinicians to personalize long-term PCa care after prostatectomy. As described above, a previous study demonstrated that HRMAS ^{1}H MRS can serve as such a tool of detection and prediction by constructing canonical scores from spectra of intact PCa tissue (139). At the same time, spermine has been demonstrated to be a potent endogenous inhibitor of PCa and tissue spermine levels may be linked to tumor aggressiveness and BCR. From these insights, the present study derives two major hypotheses.

1.4.1 Primary hypothesis

As spermine appears to serve as an inhibitor of PCa, we would expect that this is reflected in the polyamine pathway enzymatic profiles of intact PCa tissue samples. The primary objective of the present study is to detect differences in enzymatic levels in PCa tissue that can distinguish cases of BCR from non-recurrent cases. The associated null hypothesis is: There is no difference in polyamine pathway enzyme levels between cases of BCR and non-recurrent cases of PCa.

In addition to testing for statistical significance between the two groups (recurrent and non-recurrent cases) for selected *individual* enzymes, the enzymatic data will also be used to attempt to construct a *combined* enzymatic profile. The associated null hypothesis of this subordinate objective is: There is no combination of spermine pathway enzyme levels able to distinguish between cases of BCR and non-recurrent cases of PCa.

The enzymes selected for this purpose are the two rate limiting anabolic enzymes of the polyamine pathway (ODC and AdoMetDC), the rate limiting catabolic enzyme (SSAT) and the antizyme of the first-step rate limiting enzyme ODC (OAZ).

To this set of polyamine pathway enzymes, we exploratively add a protein not part of the polyamine pathway, yet frequently associated with malignant processes: the c-Myc protein. The proto-oncogene c-Myc codes for a transcription factor that regulates and co-regulates the expression of a multitude of genes. Its mutation is associated with cell proliferation in a variety of cancer types (167, 168). The collective list of enzymes chosen is presented in Table 2.

Protein	Function	Pathway	Metabolic role	Limiting
ODC	Enzyme	Polyamine pathway	Anabolic	Yes
AdoMetDC	Enzyme	Polyamine pathway	Anabolic	Yes
SSAT	Enzyme	Polyamine pathway	Catabolic	Yes
OAZ	Enzyme	Polyamine pathway	Catabolic	No
c-Myc	Transcription factor	N/A	N/A	N/A

Table 2 Proteins chosen for quantification and their physiological functions.

1.4.2 Secondary hypothesis

As shown in the preceding study, metabolomic profiles based on HRMAS ^{1}H MRS of intact PCa tissue can effectively differentiate between BCR and non-recurrent cases using specimens from the time of prostatectomy (139). If spermine functions as an endogenous inhibitor of PCa and spermine pathway enzyme levels are significantly different between PCa BCR cases and non-recurrent cases (primary hypothesis), then we secondly hypothesize that the enzymatic profile of the spermine pathway may serve to explain differences in HRMAS ^{1}H MRS metabolomic profiles. The associated null hypothesis is: There is no correlation between levels of polyamine pathway enzymes and NMR spectral region intensities. Again, this hypothesis is tested both for each individual enzyme and for combinations of various enzyme levels.

Testing this secondary hypothesis is, in short, a direct follow-up to the previously published study (139). It attempts to match and explain metabolomic profiles based on HRMAS ^{1}H MRS with enzymatic profiles based on quantitative methods of molecular biology.

2 Materials and methods

2.1 Study design and patient population

The present study is designed as a retrospective study of 32 male patients that had undergone radical prostatectomy at Massachusetts General Hospital, Boston, USA. The study of human prostate specimens was approved by the Partners Human Research Committee, the Institutional Review Board at Massachusetts General Hospital.

Cases were selected ex post from a pool of 183 prostatectomy cases that had been analyzed between 2002 and 2003 using intact tissue MRS in the Radio-pathology laboratory of the Athinoula A. Martinos Center for Biomedical Imaging, a joint research facility of Harvard Medical School and the Massachusetts Institute of Technology, Cambridge, USA. Needle biopsy specimens recovered for histopathological assessment at time of prostatectomy served as the original specimens of each case. The retrieval of the prostate tissue specimens followed current standard diagnostic biopsy protocols, with multiple samples per prostate and patient, distributed representatively across the organ.

A first group of patients (n=16) was identified based on demonstrated BCR: a PSA serum increase to >0.2 ng/ml after prostatectomy, confirmed by at least one subsequent test. To this first group of recurrent cases, a randomized selection of 16 non-recurrent cases was added from the pool of 183 prostatectomy cases. For the cases of this control group, no PSA had been detected in serum tests during the observation period.

Where multiple spectroscopy results for an individual patient were found in the pool of 183 prostatectomy cases, the results of the individual MRS scans were averaged for each patient.

Recurrent and non-recurrent cases (n=32) were matched based on age, GS, clinical staging, time lag to BCR (recurrent group) and length of observation interval (non-recurrent group). Average patient age at the time of prostatectomy was 55.3, with a standard deviation of 8.7 years. Average serum PSA concentration at the time of first detection for the recurrent group was 0.69 ng/ml. First PSA detection for this group occurred, on average, 28.5 months post prostatectomy. The average observation period without detectable serum PSA levels for the non-recurrent cases in the control group was 55.6 months. Details for the individual cases including GS and clinical staging are presented in Table 3.

Group	Pair	Age	Clinical Stage	Gleason Score	Period (months)	PSA (ng/ml)
Recurrent	1	50	1c	3 + 3 = 6	18.0	0.30
	2	51	1c	3 + 3 = 6	41.0	0.21
	3	67	1c	3 + 3 = 6	53.0	0.26
	4	51	1c	3 + 4 = 7	19.0	0.40
	5	54	1c	3 + 4 = 7	3.0	2.90
	6	57	1c	3 + 4 = 7	47.0	0.30
	7	41	1c	3 + 3 = 6	59.0	0.22
	8	50	1c	3 + 4 = 7	2.0	0.70
	9	57	1c	3 + 4 = 7	24.0	0.30
	10	62	1c	4 + 3 = 7	44.0	3.70
	11	52	1c	3 + 3 = 6	45.0	0.37
	12	55	1c	4 + 3 = 7	63.0	0.24
	13	62	1c	3 + 5 = 8	22.0	0.30
	14	66	1c	4 + 3 = 7	9.0	0.30
	15	23	2	3 + 3 = 6	0.5	0.21
	16	60	2	3 + 5 = 8	7.0	0.30
Non-recurrent	1	50	1c	3 + 3 = 6	57.0	<0.20
	2	51	1c	3 + 3 = 6	60.0	
	3	55	1c	3 + 3 = 6	59.0	
	4	51	1c	3 + 3 = 6	60.0	
	5	54	1c	3 + 3 = 6	60.0	
	6	58	1c	3 + 3 = 6	60.0	
	7	51	1c	3 + 3 = 6	59.0	
	8	60	1c	3 + 4 = 7	24.0	
	9	59	1c	3 + 3 = 6	60.0	
	10	55	1c	3 + 4 = 7	60.0	
	11	52	1c	3 + 3 = 6	60.0	
	12	62	1c	3 + 4 = 7	60.0	
	13	62	1c	3 + 4 = 7	44.0	
	14	59	1c	4 + 5 = 9	44.0	

	15	56	2	3 + 3 = 6	57.0
	16	75	2	3 + 4 = 7	65.0

Table 3 Clinical characteristics of patient population. The column 'age' lists the respective age at time of prostatectomy. The column 'period' lists the time gap between prostatectomy and first PSA increase for the recurrent group, and the total observation period after prostatectomy for the non-recurrent group, during which no PSA increase has been detected after prostatectomy.

From this group of 32 prostatectomy cases for which radiological MRS data had been available, 50% of the matched pairs (recurrent/non-recurrent) were randomly selected for molecular biological analysis using quantitative real time polymerase chain reaction (qPCR). These cases constitute a subgroup of the original patient population with $n_{total} = 16$, $n_{recurrent} = 8$ and $n_{non\text{-}recurrent} = 8$. Analogous to the original study population, BCR cases in the subpopulation remain matched to control cases by age, GS, clinical staging, time lag to BCR (recurrent group) and length of observation interval (non-recurrent group).

In the subgroup selected for qPCR, average patient age at the time of prostatectomy was 54.8, with a standard deviation of 6.5 years. Average serum PSA concentration at the time of first detection for the recurrent group was 0.69 ng/ml. First PSA detection for the group occurred, on average, 19.9 months post prostatectomy. The average observation period without detectable serum PSA levels for the non-recurrent cases in the control group was 55.8 months. Details for the individual cases in the subgroup including GS and clinical staging are presented in Table 4.

Group	**Pair**	**Age**	**Clinical Stage**	**Gleason Score**	**Period (months)**	**PSA (ng/ml)**
Recurrent	1	50	1c	3 + 3 = 6	18.0	0.30
	2	51	1c	3 + 3 = 6	41.0	0.21
	4	51	1c	3 + 4 = 7	19.0	0.40
	5	54	1c	3 + 4 = 7	3.0	2.90
	8	50	1c	3 + 4 = 7	2.0	0.70
	9	57	1c	3 + 4 = 7	24.0	0.30

	11	52	1c	3 + 3 = 6	45.0	0.37
	16	60	2	3 + 5 = 8	7.0	0.30
Non-recurrent	1	50	1c	3 + 3 = 6	57.0	<0.20
	2	51	1c	3 + 3 = 6	60.0	
	4	51	1c	3 + 3 = 6	60.0	
	5	54	1c	3 + 3 = 6	60.0	
	8	60	1c	3 + 4 = 7	24.0	
	9	59	1c	3 + 3 = 6	60.0	
	11	52	1c	3 + 3 = 6	60.0	
	16	75	2	3 + 4 = 7	65.0	

Table 4 Clinical characteristics of patient sub-population. 50% of the main population from the preceding MRS study were selected to supplement MRS data with enzymatic data for this sub-population. The column 'age' lists the respective age at time of prostatectomy. The column 'period' lists the time gap between prostatectomy and first PSA increase for the recurrent group, and the total observation period after prostatectomy for the non-recurrent group, during which no PSA increase has been detected after prostatectomy.

To test the hypotheses described above, the present study is designed to combine quantitative methods of magnetic resonance radiology with quantitative methods of molecular biology. As described above, the radiological data is based on previous HRMAS ^{1}H MRS scans of the specimens. The molecular biology enzymatic data, in contrast, has been collected specifically for the purposes of the study.

Each sample underwent four distinct methodological steps: (1) HRMAS ^{1}H MRS; (2) first histopathological assessment; (3) second histopathological assessment; (4) laser capturing microdissection (LCM) and subsequent quantitative real time polymerase chain reaction (PCR). The first histopathological assessment took place after the HRMAS ^{1}H MRS scans of 2002 to 2003 to estimate certain quantitative parameters of the specimens, such as volume percentage of epithelial and stroma cells. Details are discussed below. The second histopathological assessment, in contrast, took place in 2008 and 2009 to prepare cell targeting and extraction via LCM for qPCR. Note that the order of discussion below follows the analytic logic of the study, not its chronological order.

2.2 Histopathological assessment

All samples of the study underwent histopathological evaluation by a pathologist. Frozen samples (-80 °C) were sectioned at 10 µm cuttings using a cryostat (*CM 3050 Cryostat, Leica*, USA) producing slides for subsequent staining (*Gold seal slides - uncharged, Thermo Fisher Scientific*, USA). In total, 18 cuts per sample were produced. The protocol used for hematoxylin and eosin staining (HE) is presented in Table 5.

Step	Substrate	Time	Number of dips
1	Xylene	12 min	-
2	100% ethanol	4 min	-
3	95% ethanol	2 min	-
4	Double distilled water	-	1 (rinse)
5	Hematoxylin	5 min	-
6	Double distilled water	-	1 (rinse)
7	Bluing reagent	-	15
8	Double distilled water	-	1 (rinse)
9	95% ethanol	-	10
10	Eosin	3 min	-
11	95% ethanol	-	10 to 15
12	95% ethanol	-	10 to 15
13	100% ethanol	-	10 to 15
14	100% ethanol	-	10 to 15
15	Xylene	≥ 2 min	-

Table 5 Hematoxylin–eosin staining protocol. Staining protocol used for the histopathological assessment.

Histopathological assessment served two purposes. Firstly, in the histopathological session following HRMAS ^{1}H MRS, the pathologist estimated a series of quantitative parameters for each specimen to be used in the analysis. These were: Volume percentage of benign epithelial cells, volume percentage of malignant epithelial cells and volume percentage of stroma.

Secondly, in the histopathological session preceding LCM and qPCR, the pathologist differentiated epithelial from stroma tissue, and subcategorized the epithelial tissue further into predomi-

nantly benign and predominantly malignant regions. Typical examples exhibiting different growth patterns are given in Figure 5.

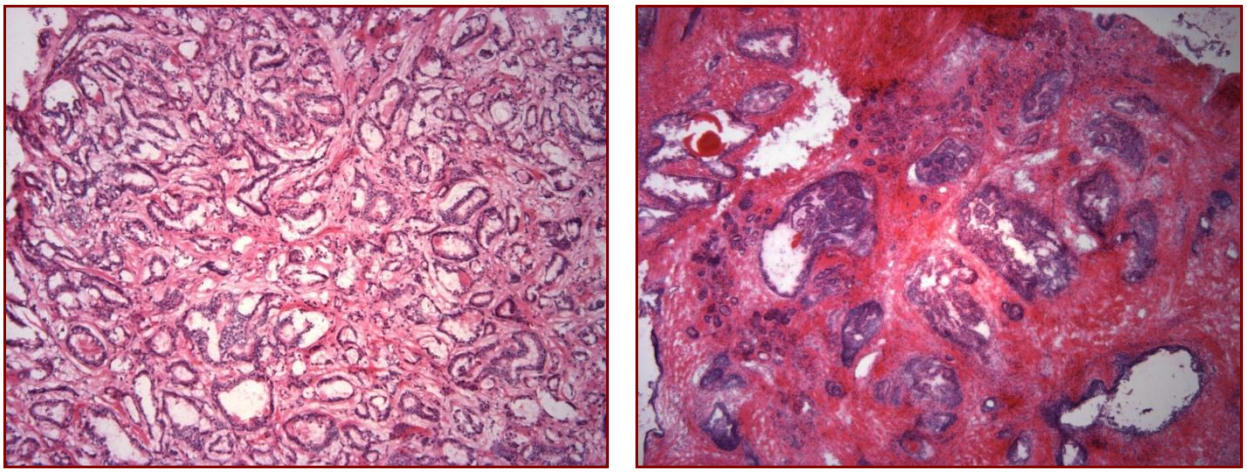

Figure 5 Tissue samples after HE-staining. Displayed are two samples of prostate tissue exhibiting predominantly malignant growth patterns, featuring one highly proliferative exhibit (left) and one moderately proliferative exhibit (right). Pictures were taken using an Olympus BX41 Microscope and Imaging System at a ten-fold magnification.

Note that ‘benign’ and ‘malignant’ here refer to the chief histological growth pattern on the specific slides cut from the specimens. All specimens as a whole stem, of course, from cancerous prostates. In this aggregate sense, all samples are to be considered malignant.

The individual cuts on the individual slides typically fell into either the benign or malignant growth pattern group, not both. And typically, each slide contained both epithelial and stroma tissue areas. This allowed us to also distinguish between stroma neighboring epithelial tissue of a predominantly benign growth pattern from stroma neighboring epithelial tissue of a predominantly malignant growth pattern.

Note that in so far as stroma is in the following labeled ‘benign’ or ‘malignant’, we here refer to the predominant growth pattern of its neighboring epithelial tissue, not the dignity of the stroma tissue itself. As PCa originates from epithelial cells, all stroma tissue in this study is in the histopathological sense ‘benign’, and none ‘malignant’. We use the biopathohistologically simplified terminology here to ease communication.

Whenever possible, we strove to identify tissue samples from each of the four sub-categories for each case. This means that, for each of the 16 PCa cases, we processed tissue samples from (1) the 'benign epithelium' category, (2) the 'malignant epithelium' category (3) the 'benign stroma' category and (4) the 'malignant stroma' category. Ideally, this would add to 4 x 16 = 64 samples entering qPCR. *De facto*, we were unable to achieve this target for some of the cases. In each case, this was due to one or more of the following reasons: (a) limited total specimen material; (b) excessively malignant growth patterns across the specimen, driving out benign epithelium; (c) excessive epithelial proliferation across the specimen, driving out stroma tissue. For some of the subgroup analyses, this drastically limited the number of samples entering statistical analysis, often thrusting results into statistical insignificance.

Depending on the specific question at hand, subgroup sample values for each case were either averaged before statistical processing or entered split statistical procedures separately. Details are explicated in this chapter below (section on statistical analysis) and sufficiently denoted in the results section.

Information from the second histopathological assessment, i.e. the classification of tissue types, was indispensable for the subsequent LCM. LCM enables one to target specific tissue, even specific cells, in each histological cut. The laser separates these individual cells or tissue sections from the tissue context as a whole on each slide. If the targeted cells are pooled, enzyme mRNA for specific cell and tissue types can be quantified by qPCR, separately from the neighboring tissue on the cut in the slide. The function of the second histopathological assessment, in short, was to mark specific targets for LCM. Technical details of LCM are discussed in the qPCR section.

2.3 Quantitative methods

2.3.1 HRMAS ^{1}H MRS

Spectroscopy was performed using an AVANCE system (*Bruker Biospin*, USA) with an MAS speed of 600~700 Hz. The system operates at 600 MHz ^{1}H frequency and 14.1 Tesla. The rotor used was a 4-mm rotor with Keel-F inserts creating a spherical space of 10-ml fixing the tissue to the center of the receiving coil. The permanently-attached external standard (silicone rubber) functioned as a reference both for resonance identification and quantification.

Recording of the spectra used a rotor synchronized DANTE Carr-Purcell-Meiboom-Gill (CPMG) pulse sequence experimental protocol. The 90° pulse length was adjusted for each sample. Resonance frequency was centered on the H_20 resonance. The spinning frequencies used were 600 and 700 Hz, the repetition time 5 sec, and the average number of transients 32, ranging from 16 to 64, with a spectral width of 12 kHz and 16 k data points.

Specimens were weighed before HRMAS ^{1}H MRS and then transferred to the HRMAS sample rotor. Samples were treated with deuterium oxide (D_2O, 2µl) for field locking. Measurements were carried out at 4°C minimizing tissue degradation during HRMAS ^{1}H MRS. For each sample, total measurement time was less than 6 minutes, total testing time less than 20 minutes.

Processing spectroscopy data included a series of steps, starting with subjecting all free induction decays to 1 Hz apodization. Fourier transformation, baseline correction and phase adjustment followed the apodization. The intensities referred to in the following are integrals of intensity curves. The curves were fitted using Lorentzian-Gaussian line shapes (137). The spectral region considered was 0.5 to 4.5 ppm. The intensity values used in subsequent statistical analyses are relative intensities with individual peaks normalized relative to the intensity of the entire spectrum between 0.5 and 4.5 ppm. All processing of spectroscopy data was done using the commercially available software *NUTS* (*AcornNMR*, USA).

2.3.2 QPCR

2.3.2.1 Overview

To quantify the enzyme levels ODC, AdoMetDC, SSAT and OAZ and the level of c-Myc, we chose the method of quantitative real time polymerase chain reaction (qPCR). This approach is based on the assumption that enzyme activity and concentration in a cell is proportional to the concentration of the corresponding messenger ribonucleic acid (mRNA) found in the cells. The mRNA concentration is in turn assumed to be proportional to the rate of expression of the genes coding for these proteins. In short, the assumption is that relative differences at the start of protein synthesis lead to matching relative downstream effects along the way of protein synthesis. Potential criticisms of qPCR as a method will be addressed in the discussion section.

The method of qPCR from human tissue samples requires a series of technical steps of isolation, synthesis and quantification, namely (1) LCM, (2) mRNA extraction, (3) complementary deoxy-

ribonucleic acid (cDNA) synthesis ('transcription') and (4) amplification using quantitative real-time polymerase chain reaction, the step lending its name to the procedure as a whole. All steps will be discussed in more detail in the following section.

To monitor and, if necessary, improve each step of the process we introduced various measures of quality control, which will also be discussed in more detail below. In short, we (a) verified primer quality and methodological accuracy based on serial dilution sequences in a pilot study, (b) used a scheme of positive and negative controls for the steps of mRNA extraction, cDNA synthesis and qPCR runs, (c) conducted pretests for each sample to optimize loading concentrations, (d) and introduced a statistical analysis tool to monitor pipetting accuracy and, if necessary, prompt re-runs.

Raw data produced in qPCR has to be processed to generate quantitative results. For this processing of raw data, we chose to run two different quantification approaches in parallel: (a) a threshold/cycle-based method, and (b) an initial intensity-based method. We used two separate approaches to increase the reliability of our results. Both methods will be discussed in detail below.

Note that both the threshold/cycle-based method and the initial intensity-based method yield *relative* concentrations of mRNA only, allowing statements about differences in *relative* levels of gene expression between different experimental groups. The methodological alternative would have been a standard curve method allowing statements to be made about *absolute* mRNA concentrations in each sample and about averages of *absolute* concentrations for the experimental subgroups. Since, for the purposes of the study, we were solely interested in relative differences between experimental groups, the relative quantification methods were deemed sufficient.

2.3.2.2 LCM

Laser capturing microdissection (LCM) allowed us to target specific cell populations and to minimise mRNA from other tissue types in the subsequent quantification process. In LCM, tissue sections or individual cells are extracted by a laser, which melts a thermoplastic film onto the targeted tissue. The thermoplastic film is mounted on LCM caps (*CapSure Macro LCM caps*, *Arcturus Engineering*, USA), which, when withdrawn, extract the tissue.

For laser capturing microdissection (LCM), slides containing frozen sections of 10 µm were fixated according to a HE quick staining protocol (Table 6), RNAse treated and air-dried.

Step	Substrate	Time (min)
1	75% ethanol	1.0
2	Purified, distilled water	2.0
3	Hematoxylin-eosin	2.0
4	75% ethanol	0.5
5	95% ethanol	2.0
6	100% ethanol	1.0
7	Xylene	5.0

Table 6 HE quick staining protocol. Protocol used before laser capturing microdissection.

The system used for LCM was a PixCell II Laser Capture Microdissection System (*Arcturus Engineering*, USA). No longer than 30 minutes were allowed for each session and no more than 3 sections were processed during any one session. For each sample, 5000 pulses were applied on average, varying with tissue type targeted and quality of the tissue on the slide. The parameters used for LCM were 35 MW laser power, 4.5 msec pulse duration and 7.5 µm spot size.

2.3.2.3 Extraction of mRNA

Pooled cell and tissue material from LCM was treated with lysis buffer to free mRNA from cell structures and other cell substrates. The mRNA was subsequently extracted through a series of extraction steps, the general principle of which is to bind polar mRNA to a polar filter while washing off unwanted non-mRNA cell material with salt buffer.

The individual steps of extraction were the following: Pooled cell material for each sample was stored in Beta-ME-Lysis Buffer and 80 µl of 70% ethanol was added. The mixture was pipetted onto a filter and spun for 1 min. 600 µl of low salt buffer was added and the mixture again spun

for 1 min. After this and each of the following spinning cycles the filtrate containing unwanted non-mRNA material was discarded, with the target mRNA trapped in the filter. Next, the filter was treated with 5 µl of DNAse and 25 µl of DNAse buffer and incubated for 15 min at 37°C. 500 µl of high salt buffer was applied to the filer and the tube spun for 1 min. In a third cycle, 600 µl of low salt buffer was applied and the tube spun for 1 min. In a fourth cycle, 300 µl of low salt buffer was pipetted onto the filter and the tube spun for 2 min. Finally, 30 µl of elution buffer was applied to the filter, separating the mRNA from the filter.

2.3.2.4 Synthesis of cDNA

For transcription, a murine leukemia reverse transcriptase was used, creating cDNA matching the extracted mRNA. All reagents were first incubated at 37°C for 1 hr, then at 95°C for 5 min. All reagents used in extraction and transcription, including the manufacturers chosen are listed in Table 7.

Product	Manufacturer
Desoxynucleosid triphosphate (DNTP)	Roche, Germany
Dithiothreitol (DTT)	Promega, USA
Primers	SABiosciences, USA
Random hexamers	Roche, Germany
Reverse transcriptase	Invitrogen, USA
RNA extraction kit	Stratagene, USA
RNAse inhibitor for cDNA	Promega, USA

Table 7 Reagents used in RNA extraction and cDNA synthesis.

2.3.2.5 Amplification by qPCR

Expression of ODC, AdoMetDC, SSAT, OAZ and c-Myc was quantified with qPCR using gene-specific primers (*SABiosciences*, USA), a fluorescence reporter (*SYBR Green Dye*, *Super Array*,

USA) and an *ABI PRISM 7000 Fast LightCycler* (*Applied Biosystems*, USA). The cycling protocol used is given in Table 8.

Cycles	Duration	Temperature
1	10 min	95°C
40	15 sec	95°C
	1 min	60°C

Table 8 **Cycling protocol.** Protocol used for qPCR amplification on an *ABI PRISM 7000 Fast LightCycler*.

To compare expression across different samples, the level of expression of the specific gene of interest in the specific sample is put into relation to the expression of a reference gene in that sample. Typically, so-called housekeeping genes are chosen as internal references as their expression varies much less with cell states than the expression of the gene of interest. Current research suggests that 18s ribosomal RNA (rRNA) may be the most appropriate reference for such purposes as its level of expression is largely unaffected by cell state, dignity and other distorting factors (169, 170). The primers used for 18s rRNA and all other enzymes are listed in Table 9.

Gene Symbol	Description	Catalog No.	Refseq Accession No.	Unigene No.
N/A	18s rRNA	PPH05666E	X 03205	N/A
ODC1	ODC	PPH00987B	NM 002539	Hs.467701
AMD1	AdoMetDC	PPH01302A	NM 001634	Hs.159118
SAT1	SSAT	PPH01303A	NM 002970	Hs.28491
OAZ1	OAZ	PPH01308E	NM 004152	Hs.446427
MYC	c-Myc	PPH00100A	NM 002467	Hs.202453

Table 9 **Primers used in qPCR.** All primers were ordered from *SABiosciences* (USA).

Amplification was monitored using a *7000 System Detection Software BioAnalysis* (Version 1.2.3, *Applied Biosciences*, USA).

2.3.2.6 Quality control

2.3.2.6.1 Primer verification and proof of concept

QPCR amplifies small amounts of mRNA to detectable levels. It is based on the assumption that small differences in loading concentration before amplification are proportionally reflected in noticeable differences after amplification. To demonstrate this relation of proportionality we conducted a sequence of PCR runs with known loading concentrations. The concentrations were systematically lowered in a series of dilutions and plotted against the resulting amplification cycle at a given threshold. Results of the preliminary proof of concept study are presented at the beginning of the results section. Note that this pilot study, if successful, also elegantly demonstrates the functionality of the individual primers and the accuracy of pipetting.

2.3.2.6.2 Scheme of positive and negative controls

Each of the steps of qPCR from mRNA extraction to amplification was supplemented by a scheme of positive and negative controls. Positive controls are based on commercial mRNA for the extraction and transcription steps and on cDNA produced from commercial RNA for the amplification step. They have known input concentrations and are known to contain all substrates necessary for successful qPCR. Negative controls, on the contrary, replace the decisive substrates with distilled H_20 and are expected to produce no fluorescence in the amplification plot.

If positive controls fail, it may be due to a number of reasons, including RNAse contamination, missing or deteriorated reagents, pipetting inaccuracy, deviation from incubation protocols or technical failure of the apparatuses involved. If negative controls fail, it is typically due to DNA contamination of samples, tubes or reagents. Using a multi-level control scheme, with newly entering controls at each step, allowed us to track down technical failure or technical inaccuracies quickly and effectively. Figure 6 summarizes the scheme of positive controls.

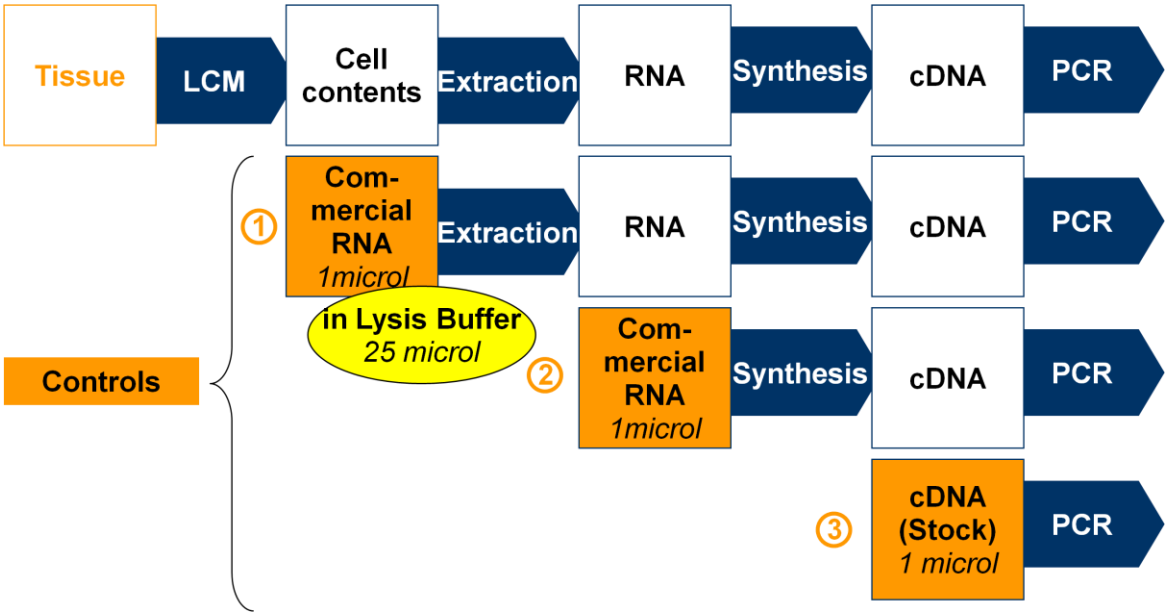

Figure 6 **Scheme of positive controls.** Each of the steps of qPCR, starting from the original tissue sample to the actual amplification process, was accompanied by a newly entering positive control. The top line portrays the procedural steps the samples underwent. The bottom three lines portray the steps each of the three positive controls underwent. Positive controls were produced either from commercially available mRNA of human prostate tissue (for the extraction and synthesis steps) or from a previously accumulated stock of cDNA (for the amplification step).

2.3.2.6.3 Pretests to optimize loading concentrations

The threshold/cycle-based quantification method relies on the assumption that amplification plots exhibit a log-linear phase during which amplification efficiency of target and reference gene are equal. In this log-linear stretch, the amplification efficiency is assumed to be equal to 2.00, i.e. perfect, across primers, across samples and across input concentrations. Figure 7 plots the amplification efficiency against the mid-cycle of the log-linear phase. It also displays enzyme groupings. Figure 7 demonstrates firstly that amplification efficiency routinely differs from the assumed optimal value of 2.00. It secondly demonstrates that amplification efficiency varies with cycle number and between enzymes, a topic of heated debate in current literature (171).

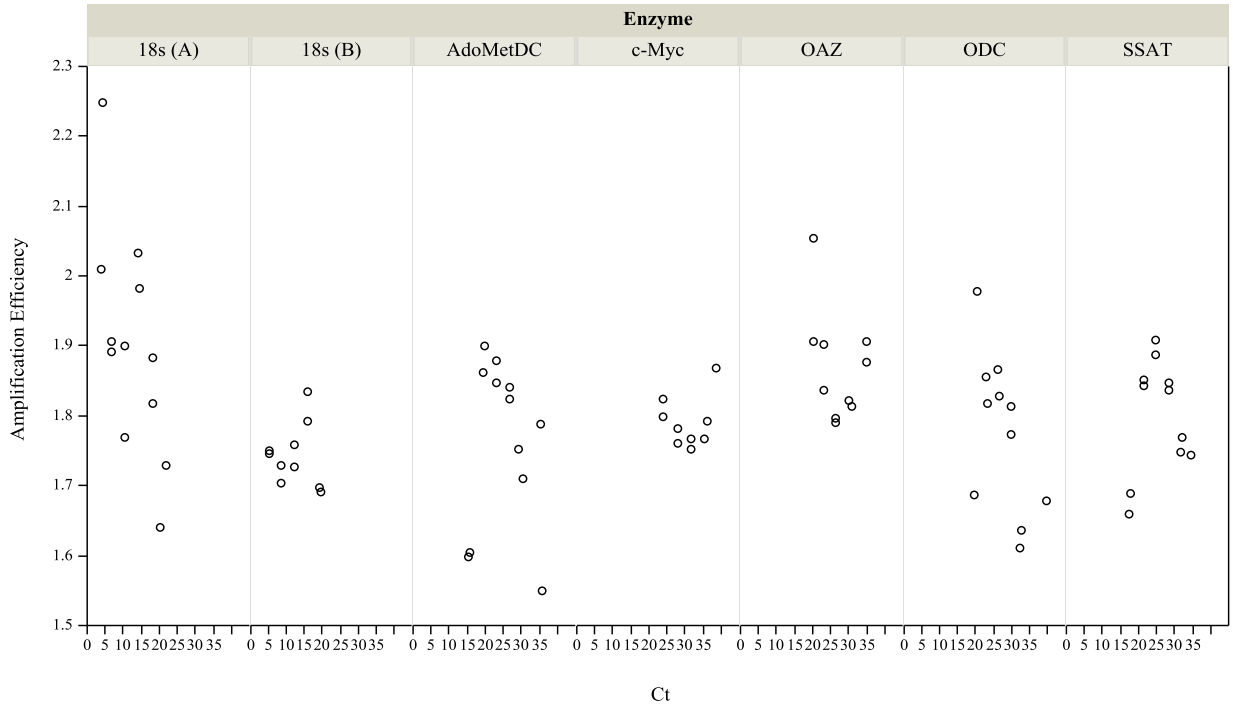

Figure 7 Amplification efficiency versus cycle by enzyme. Ct values are for a common randomly chosen threshold of the log-linear phase. The amplification efficiency routinely differs from its optimal assumed value of 2.00. The plot indicates that variation occurs both across enzymes and with entry cycle. The two variants A and B of 18s represent data from two separate qPCR runs.

In reply to these results, we performed a series of pretests before each PCR run. The pretests served to determine the input mRNA concentrations of each sample and allowed us to adjust these input concentrations by diluting or concentrating substrates. As amplification efficiency varies with input concentration, using comparable input concentrations for all the samples side-stepped an important criticism to the method. Using the initial intensity-based method of quantification, as discussed below, allowed us to counter the second criticism of the method.

2.3.2.6.4 Running technical multiples

All amplifications were performed as technical multiples. This means that, for each combination of sample, histopathological group and primer, three identical mixes entered the amplification process. Quantitative differences in amplification between these technical multiples reflect expe-

rimental error, most commonly: pipetting inaccuracies. We developed an Excel-based tool that automated the calculation of experimental error. The tool demanded re-runs where absolute min-to-max span between multiples or the standard deviations of the technical set violated certain quality thresholds. All reference genes were quantified using technical duplicates, all genes of interest using technical triplicates. Figure 8 is a screenshot of the tool.

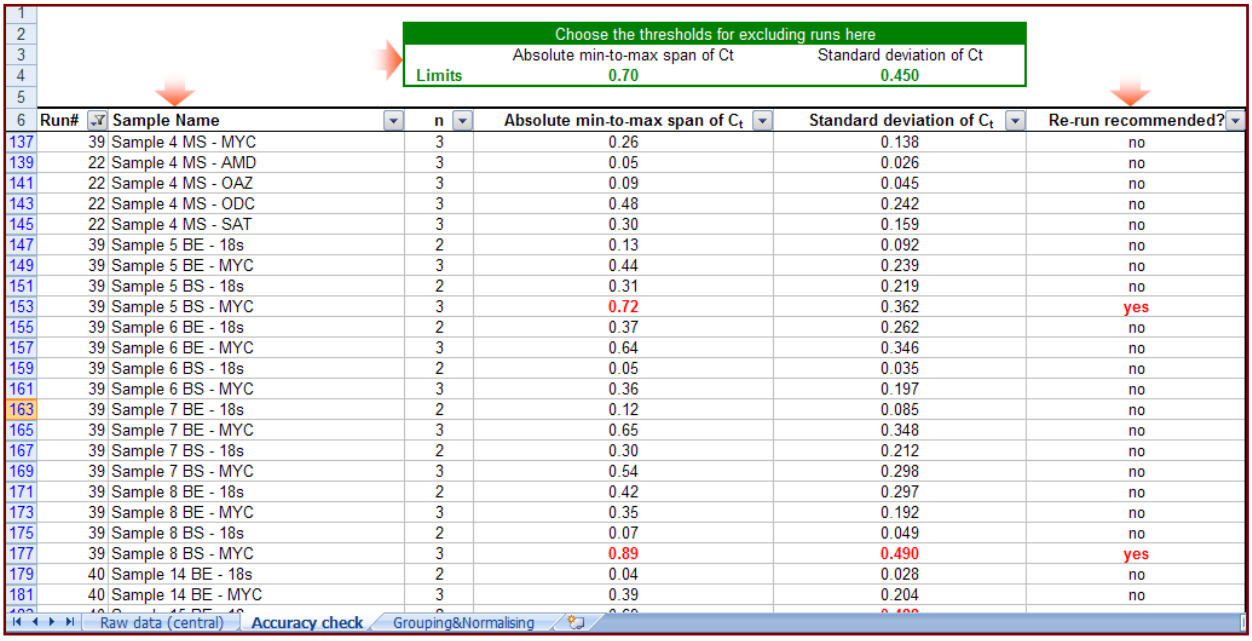

Choose the thresholds for excluding runs here

	Absolute min-to-max span of Ct	Standard deviation of Ct
Limits	0.70	0.450

Run#	Sample Name	n	Absolute min-to-max span of C_t	Standard deviation of C_t	Re-run recommended?
39	Sample 4 MS - MYC	3	0.26	0.138	no
22	Sample 4 MS - AMD	3	0.05	0.026	no
22	Sample 4 MS - OAZ	3	0.09	0.045	no
22	Sample 4 MS - ODC	3	0.48	0.242	no
22	Sample 4 MS - SAT	3	0.30	0.159	no
39	Sample 5 BE - 18s	2	0.13	0.092	no
39	Sample 5 BE - MYC	3	0.44	0.239	no
39	Sample 5 BS - 18s	2	0.31	0.219	no
39	Sample 5 BS - MYC	3	0.72	0.362	yes
39	Sample 6 BE - 18s	2	0.37	0.262	no
39	Sample 6 BE - MYC	3	0.64	0.346	no
39	Sample 6 BS - 18s	2	0.05	0.035	no
39	Sample 6 BS - MYC	3	0.36	0.197	no
39	Sample 7 BE - 18s	2	0.12	0.085	no
39	Sample 7 BE - MYC	3	0.65	0.348	no
39	Sample 7 BS - 18s	2	0.30	0.212	no
39	Sample 7 BS - MYC	3	0.54	0.298	no
39	Sample 8 BE - 18s	2	0.42	0.297	no
39	Sample 8 BE - MYC	3	0.35	0.192	no
39	Sample 8 BS - 18s	2	0.07	0.049	no
39	Sample 8 BS - MYC	3	0.89	0.490	yes
40	Sample 14 BE - 18s	2	0.04	0.028	no
40	Sample 14 BE - MYC	3	0.39	0.204	no

Raw data (central) | Accuracy check | Grouping&Normalising

Figure 8 **Accuracy control tool.** The tool analyses the experimental accuracy by calculating the absolute span between minimum and maximum values of technical multiples and their standard deviations at a given threshold. If certain accuracy limits are exceeded, the tool points out which samples should be re-run.

2.4 Data processing

2.4.1 HRMAS ^{1}H MRS

Details of HRMAS ^{1}H MRS data processing are well documented in the original publication of the preceding study (139). It was not performed by the author and is listed here for the sake of completeness only, as the present study refers to and incorporates data from this preceding study.

In a first step, the 27 most intense resonance peaks and regions were selected. The selection criterion was for the regional peak to be of greater intensity than the mean global peak of all regions analyzed. The first nine principal components were found to reflect > 85% of total variability of all intensity peaks. The first four principal components were subjected to canonical

analyses. Canonical analyses served to identify that linear combination of principal components that could best discriminate between cases of BCR and non-recurrent cases.

The canonical score thus established was subsequently tested on a second, pathological stage matched control group. Statistical tests applied included ANOVA and receiver operating characteristic (ROC) curve analyses. All statistical analyses were performed using the commercially available software *JMP 8.0* (*SAS Institute, Inc.*, USA). Details regarding the statistical methodology of the present study are discussed in a separate section (2.5) below.

2.4.2 QPCR

2.4.2.1 Threshold/cycle-based method

For the threshold/cycle-based method of quantification, the fluorescence intensity picked up by the *7000 System Detection Software* is plotted against the amplification cycle number. Figure 9 gives an example of an amplification plot. Fluorescence intensity, denoted by R_n, is plotted on the y-axis. Amplification cycle number, in the following denoted by 'C', is plotted on the x-axis. The y-axis is log-scaled, so that exponential fluorescence intensity growth appears as a linear stretch.

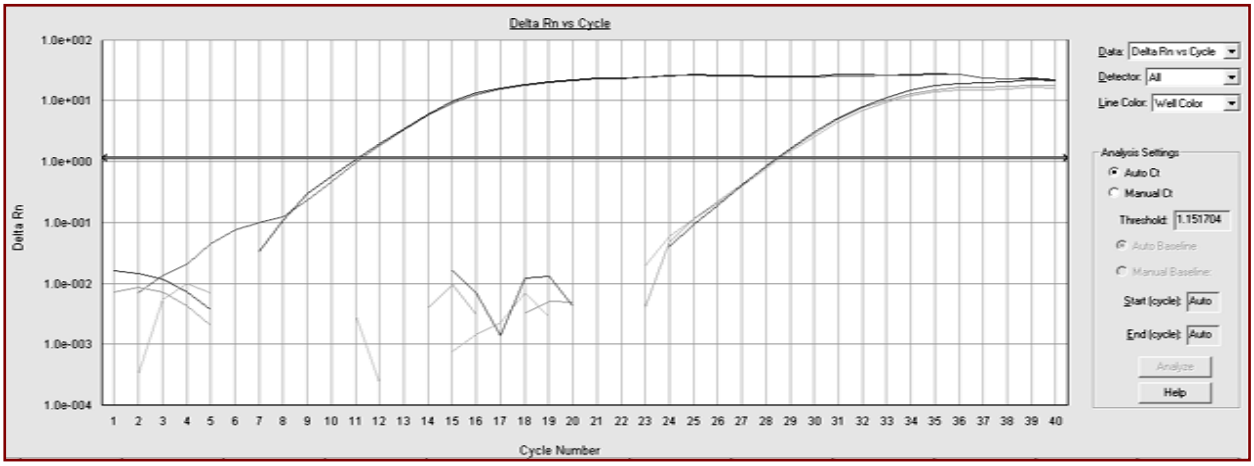

Figure 9 Example of a qPCR quantification plot. Fluorescence is plotted against cycle number. Each curve represents the amplification process of one well, i.e. of one gene in one sample. The two curves on the left are technical duplicates of the housekeeping gene (here: 18s mRNA). The three curves on the right are technical triplicates of the gene of interest (here: OAZ).

Each curve represents one sample, with congruent curves representing technical duplicates (reference gene) or technical triplicates (gene of interest) of the sample. In Figure 9, the triplet of curves to the right represents the gene of interest (target) and the duplet of curves on the left the housekeeping gene 18s (reference). Note that higher original mRNA concentrations imply that the exponential phase of quantification is reached in an earlier cycle. As the housekeeping gene concentration is several times that of the gene of interest, it kicks in on the early, left end of the x-axis, whereas the gene of interest appears much later, at the right end of the x-axis.

Quantification plots exhibit three phases: the initial exponential phase, the subsequent log-linear phase and the concluding plateau phase. Figure 10 schematically portrays the phases. The phases are also clearly visible in the example plot above (Figure 9).

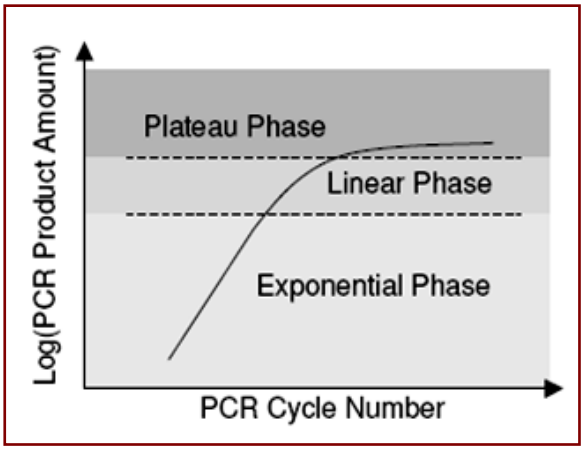

Figure 10 Schematic qPCR quantification plot.

Intensity levels in the initial phase are used for the initial intensity-based method of quantification, while intensity levels in the linear phase are used for the threshold/cycle-based approach. Note that, as qPCR is an exponential process, the second phase of the plot is linear only if the fluorescence y-axis is log-transformed.

In the log-linear phase of the amplification, the distance between the curves of reference and target gene is proportional to the mRNA input amount of reference and target. This distance between target and reference curve is defined as

$$\Delta C_t = C_t^{\text{target}} - C_t^{\text{reference}}$$

where t is any given fluorescence threshold on the y-axis that is part of the log-linear stretch of the curves and C_t the cycle number at that threshold. ΔC_t is therefore an absolute cycle difference measure. It is not an absolute measure of concentration (172).

Note that ΔC_t is independent of the threshold if and only if (a) t falls into the log-linear stretch for both curves and (b) both curves have the same amplification efficiency. On a log-scaled plot, equal amplification efficiencies in the log-linear phase are reflected as equal slopes of the curves.

To compare the expression of a gene of interest between two samples, the difference between their respective differences to their respective reference gene has to be compared. This 'difference of differences' is defined as

$$\Delta\Delta C_t = \Delta C_t\,(\text{Sample 1}) - \Delta C_t\,(\text{Sample 2})$$

where

$$\Delta C_t\,(\text{Sample 1}) = C_t^{\text{target, Sample 1}} - C_t^{\text{reference, Sample 1}}$$

$$\Delta C_t\,(\text{Sample 2}) = C_t^{\text{target, Sample 2}} - C_t^{\text{reference, Sample 2}}$$

Note that, like ΔC_t, $\Delta\Delta C_t$ is an absolute cycle difference measure, not an absolute measure of difference in concentration (173).

Since the y-axis is a logarithm 2-based transformed fluorescence signal, the following formulae apply to calculate differences in concentration between the original templates:

$$\text{Sample 1: } \frac{[c]_{target}}{[c]_{reference}} = 2^{-\Delta Ct\,(\text{Sample 1})}$$

$$\text{Sample 2: } \frac{[c]_{target}}{[c]_{reference}} = 2^{-\Delta Ct\,(\text{Sample 2})}$$

and

$$\frac{[c]_{target,\ Sample\ 1}}{[c]_{target,\ Sample\ 2}} = 2^{-\Delta\Delta Ct}$$

where $[c]_x$ is the input concentration of substrate x.

In short, ΔC_t and $\Delta\Delta C_t$ are absolute measures of cycle differences, $2^{-\Delta Ct}$ and $2^{-\Delta\Delta Ct}$ are relative measures of concentration differences (174-176). Note that, while higher values of ΔC_t imply *lower* concentrations, higher values of $2^{-\Delta Ct}$ imply *higher* concentrations (174-176). This causes the phenomenon that, depending on which parameter is chosen for an axis in a plot, the reading of the plot may be reversed.

2.4.2.2 Initial intensity-based method

The initial intensity method uses sigmoidal curve fitting to extrapolate initial fluorescence intensities from other fluorescence intensities of the amplification plot. While these later intensities are distinguishable as elements of curves, initial intensities are hidden in noise bands technically inaccessible to the plots of threshold/cycle-based methods. The simple exponential model of the log-linear phase is replaced by a sigmoidal model. Using a standard iterative process, the model fits a hypothesized curve to the data points in the amplification plot.

Modeling follows a four-parametric sigmoid function:

$$F_c = \frac{F_{max}}{1 + e^{-(c - c_{1/2}/k)}} + F_b$$

where c is the cycle number, F_c fluorescence at cycle c, F_{max} maximal fluorescence, $c_{1/2}$ the fractional cycle at which fluorescence reaches half of F_{max}, k the slope of the curve and F_b background fluorescence (177).

Differences in concentrations are then estimated from differences in extrapolated initial intensities. One of the advantages of the initial intensity-based method over threshold/cycle-based methods (if no amplification efficiency adjustments and no adjustments of input template concentrations are made) is that results are independent of amplification efficiency variations. As discussed, such variations may occur across different loading concentrations and enzymes and may even change during the qPCR amplification of an individual sample (177-179).

2.5 Statistical analysis

2.5.1 General note on statistical significance

Statistical testing for significant differences between experimental groups was conducted performing a variety of standard methods of statistics. If sample values were normally distributed, standard ANOVA analysis was used. (1-α) was set to 0.95 and p-values < 0.05 were judged statistically significant. If sample values were *not* normally distributed, the non-parametric Wilcoxon Test was used. Testing for normal distribution was performed using a Shapiro-Wilk Test estimating the goodness of fit with the normal distribution curve. Although all distributions were first plotted and Shapiro-Wilk tested, we only report the results of the appropriate Wilcoxon Tests if they produced different results (in terms of statistical significance) than standard ANOVA.

2.5.2 Specific statistical parameters

2.5.2.1 Primary hypothesis

The primary hypothesis to be tested, to recall, is the following: Polyamine pathway enzyme levels differ between cases of BCR and non-recurrent cases of PCa. The associated null hypothesis: There is no difference in polyamine pathway enzyme levels between cases of BCR and non-recurrent cases of PCa. This was formalized as statistical testing for significant differences in group mean values, applying the definition of statistical significance stated in the preceding section, and using the following parameters:

Independent variable — Clinical outcome of case

Recurrent / Non-recurrent

Dependent variable — Relative mRNA concentration in tissue sample

1a: $2^{-\Delta Ct}$ 1b: log ($2^{-\Delta Ct}$)

2a: Initial intensity 2b: log (Initial intensity)

Grouping — Tissue type

Epithelium / Stroma

Predominant histopathological growth pattern on slide

Malignant / Benign

Individual enzymes Testing the hypothesis for each individual enzyme, the dependent variable in each run was the respective group mean for each of the four selected proteins, i.e. ornithine decarboxylase (ODC), S-adenosyl-methionine decarboxylase (AdoMetDC), acetyl-CoA spermidine/spermine N1-acetyl-transferase (SSAT), and ornithine decarboxylase antizyme (OAZ).

Combinations of enzymes Testing the hypothesis for combinations of two or more of the enzymes, a multivariate model was applied. For this we chose a stepped least-squares linear fitting process. We also report the results of chi-square testing and effect likelihood ratio tests where appropriate.

2.5.2.2 Secondary hypothesis

To recapitulate, we secondly hypothesize that differences in the levels of polyamine pathway enzymes correspond to differences in HRMAS ^{1}H MRS metabolomic profiles. The associated null hypothesis has been formulated as: There is no correlation between levels of polyamine pathway enzymes and HRMAS ^{1}H MRS spectral region intensities. In terms of statistical methodology, we formalize this as the calculation of the coefficient of correlation R^2. We assume a linear relation between independent and dependent variable, again applying the definition of statistical significance stated in the preceding section, and this time using the following parameters:

Independent variable Relative mRNA concentration in tissue sample

1a: $2^{-\Delta Ct}$ 1b: log ($2^{-\Delta Ct}$)

2a: Initial intensity 2b: log (Initial intensity)

Dependent variable	HRMAS ^{1}H MRS intensity
	Normalized spectral region intensity: regional intensity relative to global intensity between 0.5 and 4.5 ppm
Grouping	Tissue type
	Epithelium / Stroma
	Predominant histopathological growth pattern on slide
	Malignant / Benign

Individual enzymes Testing the hypothesis for each individual enzyme, the respective case values for ODC, AdoMetDC, SSAT and OAZ served as the independent variable in each run.

Combinations of enzymes Testing the hypothesis for combinations of two or more of the enzymes, again, a multivariate model was applied. Here we systematically correlated linear combinations (least-squares linear fitting) of the independent variables (i.e. the relative mRNA concentration) against each of the dependent variables (i.e. the respective intensity of each HRMAS ^{1}H MRS spectral region). For each, we calculated the coefficient of correlation R^2 and ranked the models according to their respective goodness of fit.

2.6 Contributions by the author

This study brings together the material, data and work of several contributors, as in fact many studies of reasonable complexity do. For the purposes of this dissertation, it appears both necessary and appropriate to briefly demarcate the work contributed specifically by the author of the dissertation.

The steps contributed specifically and individually by the author were: (1) carrying out all aforementioned experimental 'bench' methods of molecular biology, specifically all laboratory work pertaining to qPCR; (2) developing the measures of experimental quality control as described in section 2.3.2.6; (3) developing a software tool automating the data processing de-

scribed in section 2.4.2; (4) matching qPCR data with existing MRS data; and (5) selecting and applying the appropriate statistical methodology.

Steps contributed or previously established by others and gratefully adopted for the purposes of this dissertation were: (1) carrying out all steps of tissue sample retrieval and processing; (2) carrying out all steps of histopathological assessment; and (3) carrying out the HRMAS ^{1}H MRS scans and subsequent data processing, as elaborately documented in the original publication of the preceding study (139).

3 Results

3.1 Preliminary methodological findings

3.1.1 Proof of concept of qPCR

The qPCR method amplifies small amounts of mRNA to detectable levels. As discussed at length above, it relies on the assumption that differences in substrate concentrations are proportional to differences in the fluorescence generated. Before presenting the results of the actual hypothesis testing, we therefore here first present the results of the proof of concept pilot study. The pilot study checks if the assumption of proportionality holds for qPCR.

To demonstrate the relation of proportionality, concentrations were systematically lowered in a series of dilutions. In Figure 11, these concentrations are plotted against the resulting amplification cycle at a randomly chosen threshold. The figure includes plots for all enzymes involved in the study, namely ornithine decarboxylase (ODC), S-adenosyl-methionine decarboxylase (AdoMetDC), acetyl-CoA spermidine/spermine N1-acetyl-transferase (SSAT), and ornithine decarboxylase antizyme (OAZ). Additionally, it includes the reference substrate 18s ribosomal RNA (18s) and the proto-oncogene c-Myc.

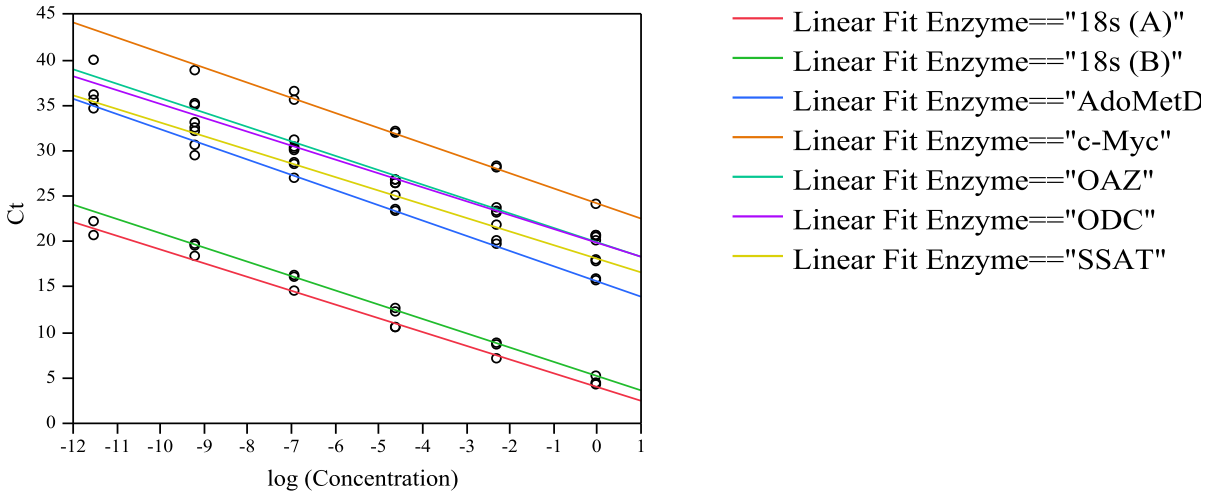

Figure 11 Linear fit of Ct and concentration (log-transformed) by protein.

Next, a linear regression analysis was performed. R^2 values for the individual enzymes ranged from 0.972 for ODC to 0.999 for the housekeeping gene 18s. Details are listed in Table 10.

Enzyme	R^2	R^2 adjusted	Root mean square error	Number of observations
18s (A)	0.9942	0.9936	0.5027	12
18s (B)	0.9995	0.9995	0.1246	10
ODC	0.9722	0.9691	1.0557	11
AdoMetDC	0.9905	0.9895	0.7044	12
SSAT	0.9973	0.9970	0.3168	11
OAZ	0.9903	0.9891	0.5737	10
c-Myc	0.9934	0.9924	0.4635	9

Table 10 Linear fit of Ct and concentration (log-transformed) by protein: R^2 square values.

3.1.2 Congruence of quantification methods for qPCR

As discussed above, we chose to use two distinct methods of quantification for qPCR, namely a threshold/cycle-based method and an initial intensity-based method. In a preliminary exercise, we evaluated the congruence of the two quantification methods using linear regression analysis. Figure 12 displays the exemplary results for ODC and AdoMetDC. Quantification results for each sample based on the threshold/cycle-based method are plotted on the y-axis, while those based on the initial intensity-based method are plotted on the x-axis. Key parameters of linear correlation analysis for ODC and AdoMetDC are listed in Table 11. R^2 Values for all enzymes ranged from 0.27 to 0.34.

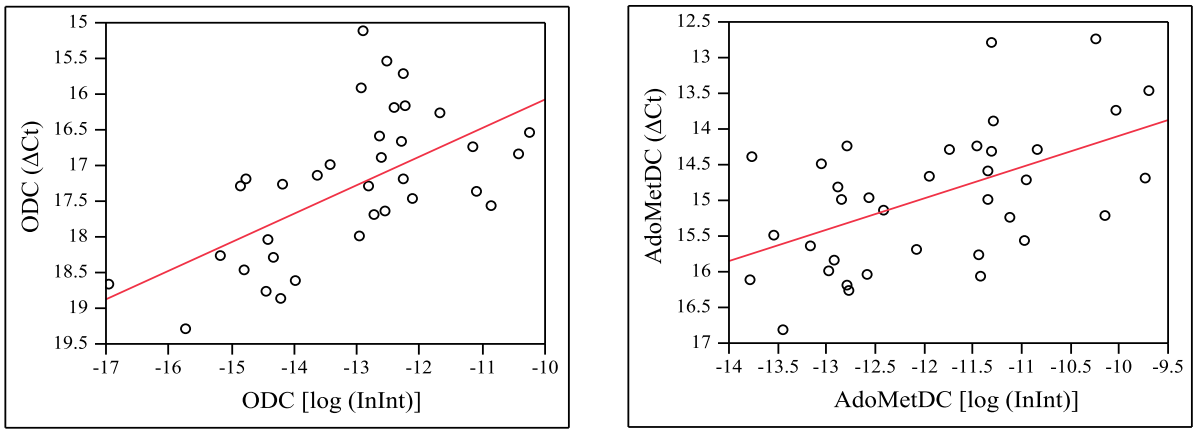

Figure 12 Bivariate fit of ΔCt by initial intensity (log-transformed) for ODC (left) and AdoMetDC (right).

	ODC	AdoMetDC
RSquare	0.338801	0.279541
RSquare Adj	0.315187	0.254698
Root Mean Square Error	0.849634	0.85295
Mean of Response	17.41056	14.98392
Observations	30	31

Table 11 ΔCt by initial intensity (log-transformed): Bivariate fit for ODC (left) and AdoMetDC (right).

Note that perfect congruence of methods would imply $R^2 = 1.00$. The coefficients of correlation found deviate considerably from this optimal value. In the few cases where statistical significance depended on the quantification method chosen, this will be reported in the following. The general implications of the deviation will be addressed in the discussion section.

3.2 Primary hypothesis

3.2.1 Individual enzymes

3.2.1.1 ODC

Analyzing the difference in gene expression of the ornithine decarboxylase (ODC) between cases of BCR and non-recurrent cases, we found that the level of ODC is generally higher in the recurrent group. Figure 13 shows the ODC level by group, once as measured by the threshold/cycle-based method and once as measured by the initial intensity-based method. $2^{-\Delta\Delta Ct}$ for benign epithelium between the groups was 1.35, which means that ODC expression in epithelial cells with predominantly benign growth pattern in patients with no prostate cancer recurrence was, on average, only 74.20% of that in patients with BCR after radical prostatectomy.

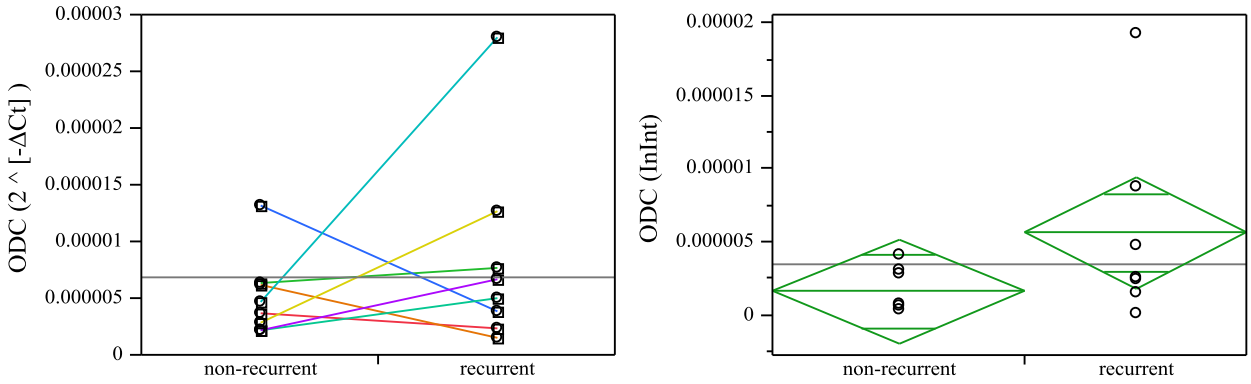

Figure 13 ODC by recurrent vs non-recurrent. Left: $2^{-\Delta Ct}$ (matched pairs); right: initial intensity.

Formal testing revealed, however, that the differences in means were not statistically significant. The results of the ANOVA are given in Table 12.

Source	DF	Sum of Squares	Mean Square	F Ratio	Prob > F
BCR	1	6.00E-11	6.01E-11	2.7844	0.1191
Error	13	2.80E-10	2.16E-11		
C. Total	14	3.40E-10			

Table 12 ODC by recurrent vs non-recurrent: Analysis of variance.

After the Shapiro-Wilk test revealed a lack of fit with the normal distribution, non-parametric testing was also performed. Table 13 lists the parameters. As Prob > |Z| was 0.5244, the null hypothesis could not be rejected.

Level	Count	Score Sum	Score Mean	(Mean-Mean0)/Std0
non-recurrent	8	53	6.625	-1.215
recurrent	7	67	9.57143	1.215

Table 13 ODC by recurrent vs non-recurrent: Wilcoxon / Kruskal-Wallis Tests (Rank Sums).

3.2.1.2 AdoMetDC

For the S-adenosyl-methionine decarboxylase (AdoMetDC), a significant difference (p = 0.0134) was found between recurrent and non-recurrent groups in terms of ΔCt of benign epithelial cells. $2^{-\Delta\Delta Ct}$, i.e. the fold difference between the groups, was calculated to be 2.26. This means that AdoMetDC expression in epithelial cells with predominantly benign growth pattern in patients with no prostate cancer recurrence was, on average, only 44.30% of that in patients with BCR after radical prostatectomy. Figure 14 plots gene expression by recurrent versus non-recurrent group. The left panel gives the results based on the threshold/cycle-based method, the right panel the results based on the initial intensity-based method. The left panel also demonstrates the relations between matched pairs of patients, the right panel visualises the analysis of variance.

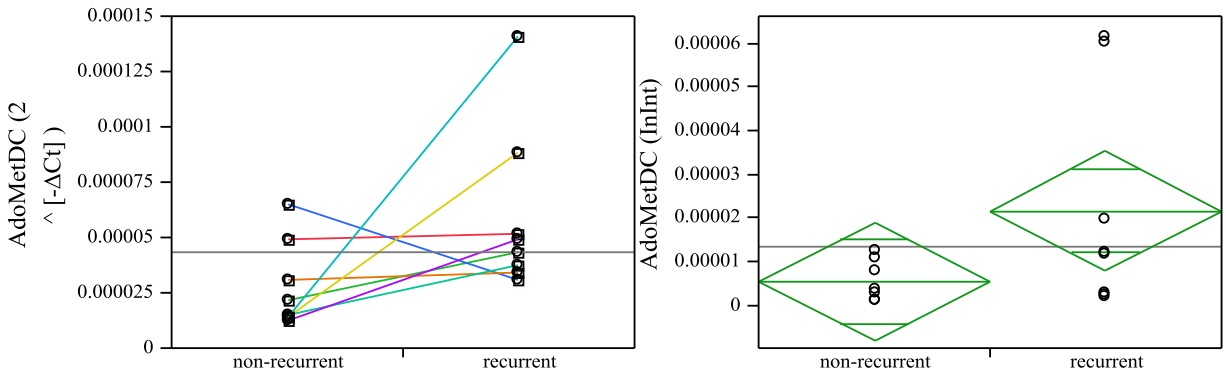

Figure 14 AdoMetDC by recurrent vs non-recurrent. Left: $2^{-\Delta Ct}$ (matched pairs); right: initial intensity.

3.2.1.3 SSAT

For the acetyl-CoA spermidine/spermine N1-acetyl-transferase (SSAT), no significant differences between the two groups were found. The fold difference in relative gene expression between recurrent and non-recurrent groups ($2^{-\Delta\Delta Ct}$) was 1.47, with an expression of 67.82% in non-recurrent patients relative to that in BCR patients. The threshold/cycle-based method delivered a p-value of 0.089 for stroma cells neighboring benign epithelium. Using the initial intensity-based method, no significant differences were detected for either epithelium or stroma. Replacing ANOVA by non-parametric tests based on a non-normal distribution improved p-values slightly, but not decisively. Figure 15 visualises the results as before.

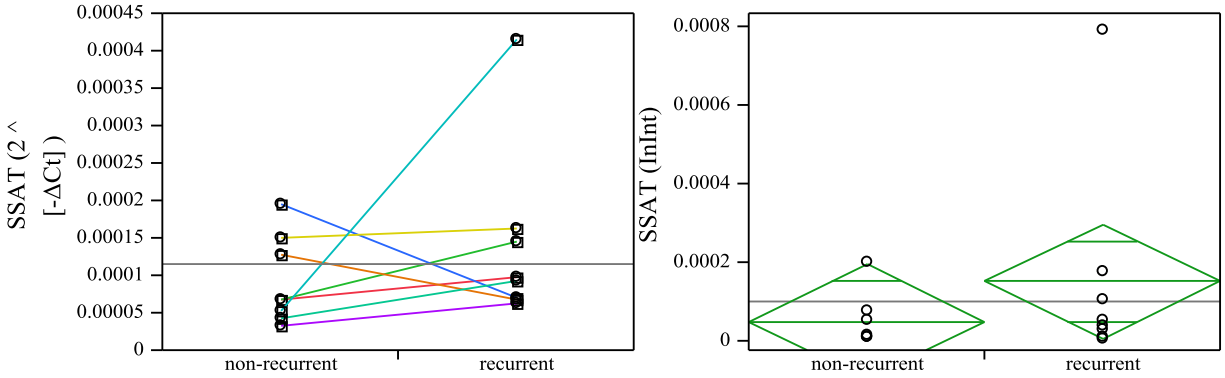

Figure 15 SSAT by recurrent vs non-recurrent. Left: $2^{-\Delta Ct}$ (matched pairs); right: initial intensity.

3.2.1.4 OAZ

A significant difference (p = 0.0252) was found between recurrent and non-recurrent groups for the log-transformed initial intensity of the ornithine decarboxylase antizyme (OAZ) expression in benign epithelial cells. For non-log-transformed initial intensity, the difference was less convincing (p = 0.0490), but still significant. $2^{-\Delta\Delta Ct}$, i.e. the fold difference between the groups, was 1.77 for epithelium and 1.69 for stroma, with a relative expression of the enzyme of 56.54% and 59.10% in non-recurrent patients when compared to BCR patients. Figure 16 plots gene expression by recurrent versus non-recurrent group. As before, the left panel gives the results based on the threshold/cycle-based method and displays the matched pairs, the right panel presents the results based on the initial intensity-based method. The left panel also demonstrates the relations between matched pairs of patients, the right panel visualises the analysis of variance. The figure

demonstrates the observation that the antizyme of the main anabolic player of spermine synthesis is more highly expressed in those patients that experience recurrence after prostatectomy than in those that do not suffer from relapse.

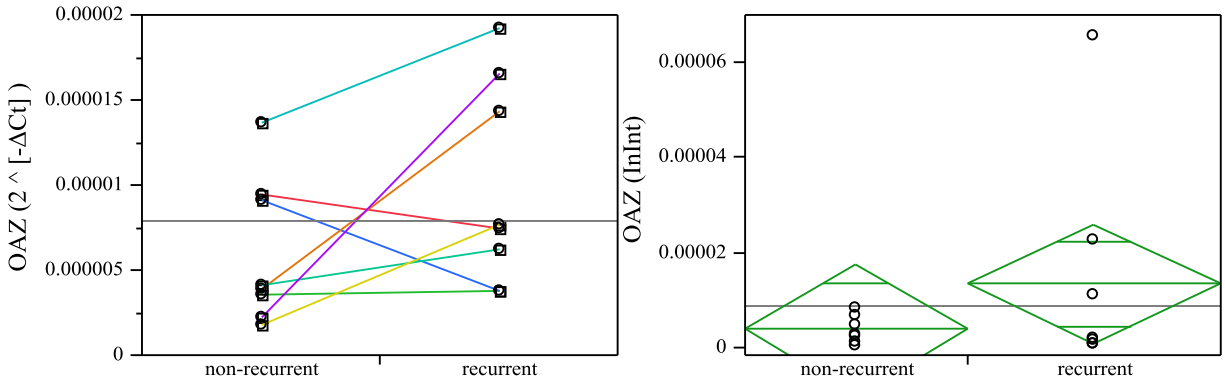

Figure 16 OAZ by recurrent vs non-recurrent. Left: $2^{-\Delta Ct}$ (matched pairs); right: initial intensity.

3.2.2 Combined model

Following the analysis of the individual enzymes of the polyamine pathway, all enzymes were combined to generate a united enzymatic profile of BCR. A least squares model was fitted to the qPCR data, with log-transformed initial intensity. Table 14 summarize the whole model test: The enzymatic profile was found to differ significantly (p = 0.0004) between recurrent and non-recurrent groups for gene expression in stroma cells. Gene expression in epithelial cells differed near-significantly (p = 0.0538).

Model	-LogLikelihood	DF	ChiSquare	Prob>ChiSq
Difference	10.36385	4	20.7277	0.0004*
Full	4.40E-08			
Reduced	10.36385			
Observations	15			

Table 14 Recurrent vs non-recurrent - combined enzyme model: Whole model test (using log-transformed initial intensity).

Of the four components of the model, i.e. ODC, AdoMetDC, SSAT and OAZ, all but AdoMetDC were found to differ significantly between the groups in the context of the linear model. Results for the gene expression in stroma cells are given in Table 15.

Source	Nparm	DF	L-R ChiSquare	Prob>ChiSq
ODC [log (InInt)]	1	1	10.15925	0.0014*
AdoMetDC [log (InInt)]	1	1	0	1
SSAT [log (InInt)]	1	1	6.052938	0.0139*
OAZ [log (InInt)]	1	1	13.80164	0.0002*

Table 15 Recurrent vs non-recurrent - combined enzyme model: Effect likelihood ratio tests (using log-transformed initial intensity).

Note that the multivariate model was generated on the basis of the two testing cohorts of this study, namely the recurrent and the non-recurrent groups of patients. It was not verified by applying it to a third cohort. The implications of this for the validity of the model will be addressed in the discussion section.

3.3 Secondary hypothesis

3.3.1 Individual enzymes

3.3.1.1 ODC

Fitting ornithine decarboxylase (ODC) gene expression data to magnetic resonance spectroscopy data from the preceding study offered only few convincing insights. Correlation coefficients were calculated for a standard least squares linear model. MRS intensity was fitted to initial intensities as exemplified by Figure 17.

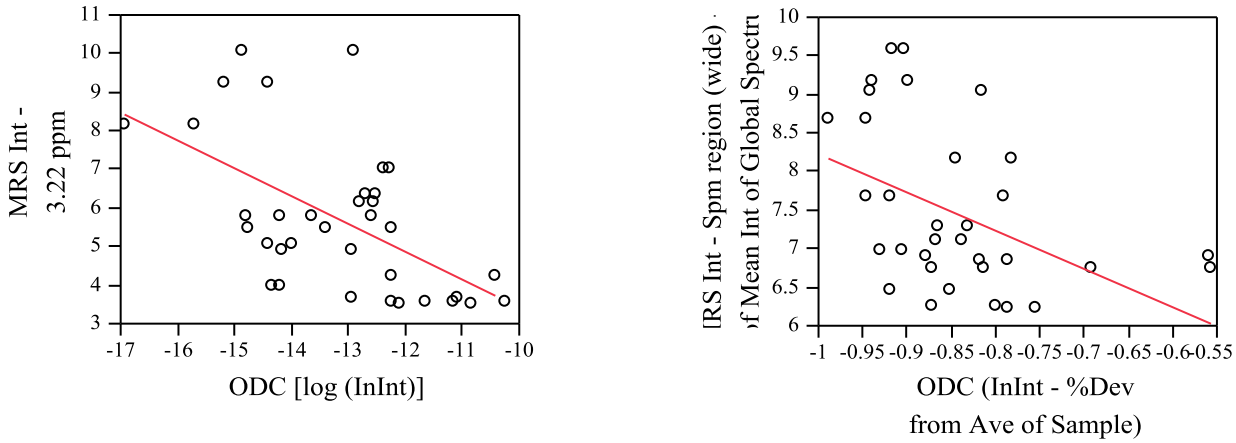

Figure 17 Linear fit of MRS intensity to ODC level: Two selected examples.

For the principal component that is the spectral region of 3.22 ppm, R^2 was 0.277 when fitted to a log-transformed initial intensity of ODC expression. A double log-transformed linear model had a fit of R^2 = 3.030. The general spectral region, in which spermine may be detected, produced a correlation coefficient of R^2 = 0.214 when the percentage deviation of the region from the global intensity was fitted to a log-transformed initial intensity of ODC. Other principal components with similar fits were 0.9 ppm (R^2 = 0.159) and 3.78 ppm (R^2 = 0.176).

3.3.1.2 AdoMetDC

Analogous to ODC, S-adenosyl-methionine decarboxylase (AdoMetDC) gene expression data was fitted to magnetic resonance spectroscopy data from the preceding study following a least squares linear model as exemplified by Figure 18.

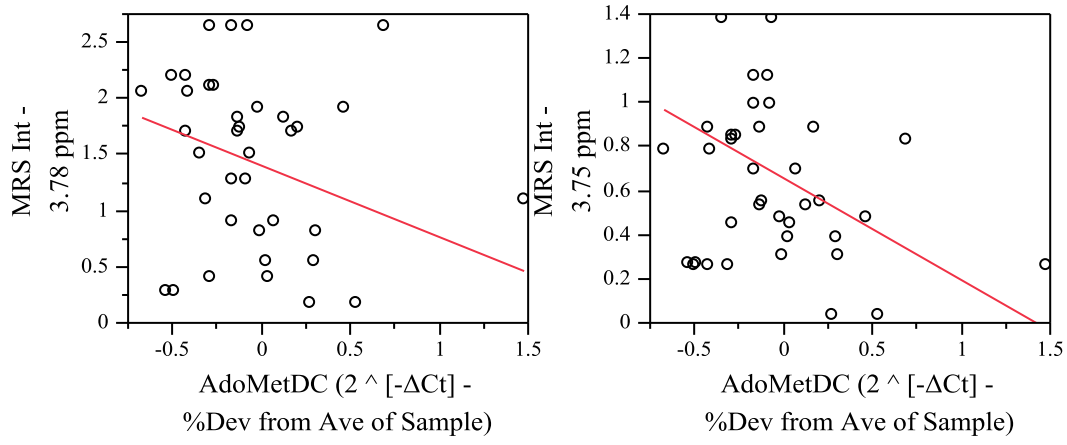

Figure 18 Linear fit of MRS intensity to AdoMetDC level: Two selected examples.

Similar to ODC, none of the correlations of AdoMetDC with the MRS principal components was entirely convincing. For the principal component that is the spectral region of 3.78 ppm, R^2 was 0.212 when fitted to the percentage deviation of ODC expression as calculated by the threshold-cycle-based method. Another principal components with a similar fit was 3.75 ppm (R^2 = 0.255). None of the other principal components reached a fit R^2 > 2.000 based on either quantification method.

3.3.1.3 SSAT

For the acetyl-CoA spermidine/spermine N1-acetyl-transferase (SSAT), too, linear fitting of spectroscopy and enzymatic data did not yield decisive results. Figure 19 exemplifies a typical correlation scenario using the two principal components of the magnetic resonance spectrum at 3.29 + 3.27 ppm and 2.45 ppm.

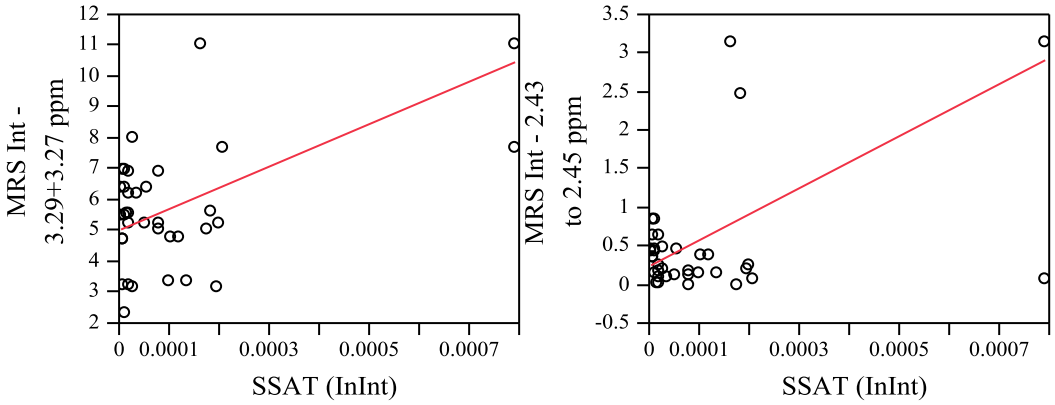

Figure 19 Linear fit of MRS intensity to SSAT level: Two selected examples.

Different from the plots above, the x-axis is here not log-scaled. This allows the observation that, for SSAT, the best nominal fits with MRS data are in fact largely based on a few outliers driving up R^2. These best fits were for the regions 2.43 to 2.45 (R^2 = 0.439) and 3.29 + 3.27 ppm (R^2 = 0.259).

3.3.1.4 OAZ

For the ornithine decarboxylase antizyme (OAZ), two of the better linear fits were detected for the principal components that are spectral region 4.11 to 4.14 ppm (R^2 = 0.133) and spectral region 3.22 (R^2 = 0.156). Both correlation coefficients are negligibly small, as demonstrated visually by the erratic scatter plots in Figure 20. The best fit was detected for the principal component that is spectral region 2.43 to 2.45 ppm to log-transformed initial intensity (R^2 = 0.366). None of the other spectral regions correlated to any significant extent.

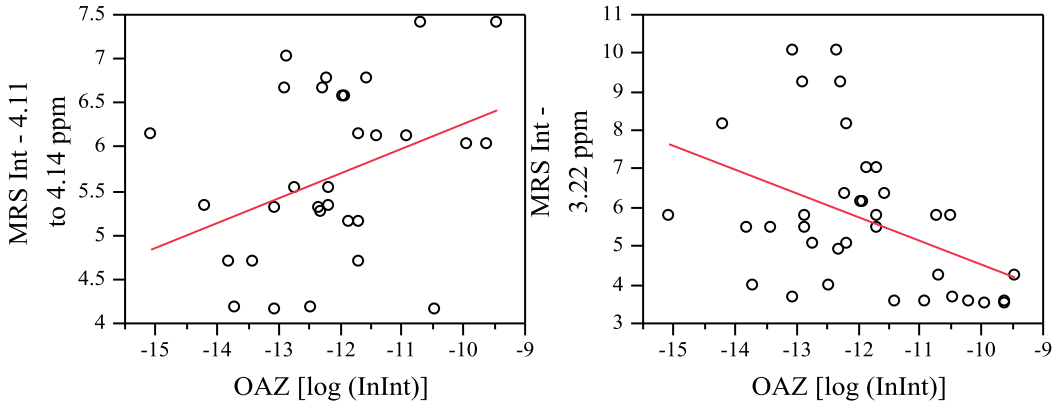

Figure 20 Linear fit of MRS intensity to OAZ level: Two selected examples.

3.3.2 Combined model

Besides correlating individual enzymes with individual principal components of the resonance spectrum, a second and alternative approach is the combination of several enzymes in one model. Linear combinations of the enzymatic expression levels were plotted against magnetic resonance intensity. This means that an enzymatic profile established by means of a molecular biological method, namely qPCR, was fitted to a metabolomic profile established by means of a radiological method, namely, HRMAS ^{1}H MRS. Table 16 presents some of the top correlations found for linear combinations of selected enzymes.

MRS principal component	Enzymes included as factors	Quantification method	R^2
2.43 to 2.45 ppm	ODC, AdoMetDC, SSAT, OAZ	Initial intensity	0.823
3.29 + 3.27 ppm	ODC, AdoMetDC, SSAT, OAZ	Initial intensity	0.571
3.75 ppm	ODC, AdoMetDC, SSAT, OAZ	$2^{-\Delta Ct}$	0.461
2.43 to 2.45 ppm	ODC, AdoMetDC, SSAT	Initial intensity	0.437
3.75 ppm	ODC, AdoMetDC, SSAT	$2^{-\Delta Ct}$	0.411
3.26 + 3.24 ppm	ODC, AdoMetDC, SSAT, OAZ	Initial intensity	0.406
3.22 ppm	ODC, AdoMetDC, SSAT, OAZ	$2^{-\Delta Ct}$	0.393
3.22 ppm	ODC, AdoMetDC, SSAT	$2^{-\Delta Ct}$	0.327
3.29 + 3.27 ppm	ODC, AdoMetDC, SSAT	Initial intensity	0.321

Table 16 Linear fit of MRS intensity to enzymatic profile: Top nine correlations found.

Table 16 indicates that an integrated enzymatic profile delivers a decisively better fit with MRS metabolomic profiles. Note that the correlation coefficients given refer to linear modeling only. Non-linear models were not systematically examined in this study. In so far as non-linear models were examined tentatively and exploratively, it yielded some noteworthy results. The principal component that is the spectral region 3.29 + 3.26 ppm, for example, correlates with $R^2 = 0.411$ when fitted linearly to an ODC/SSAT/OAZ combination. When a third degree polynomial function is applied, however, the coefficient of correlation R^2 for the now non-linear model is 0.810, i.e. a drastically tighter fit.

It is also noteworthy that the multivariate models presented here were again generated on the basis of the two testing cohorts of this study only, i.e. the recurrent and the non-recurrent groups of patients. Again, the implications of not applying the models to a third cohort will be addressed in the discussion section.

3.4 Additional findings

3.4.1 c-Myc

The expression of c-Myc was found not to differ significantly between the recurrent and the non-recurrent groups. This was true for both epithelial and stroma tissue and for both threshold/cycle-based results and initial intensity-based results. Figure 21 demonstrates the results for stroma cells. Note how the spread of ΔCt-values is much greater among recurrent cases than among non-recurrent ones. The group mean does not differ perceivably, however.

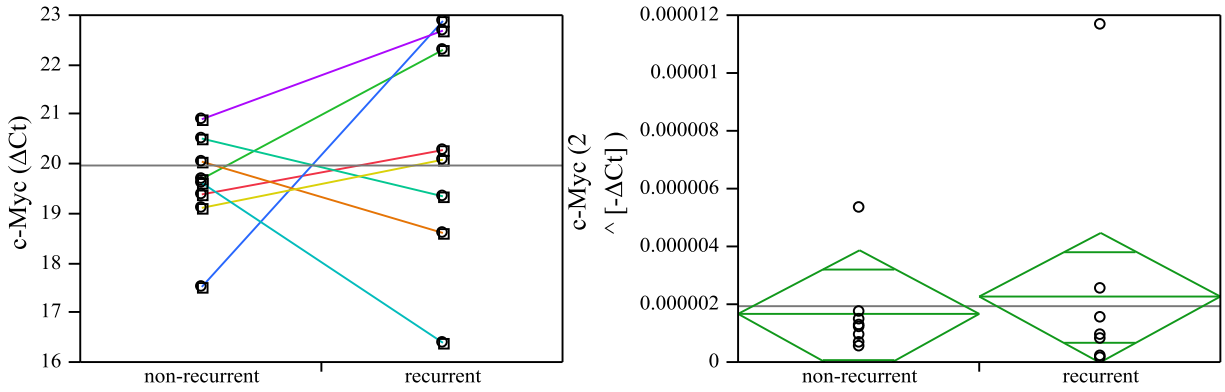

Figure 21 C-Myc by recurrent vs non-recurrent. Left: $2^{-\Delta Ct}$ (matched pairs); right: initial intensity.

3.4.2 Correlation of anabolic enzymes

In addition to the results discussed so far, we observed that across all types of tissue and across the recurrent / non-recurrent divide, anabolic enzymes appear to be regulated in parallel. An up-regulation of ODC implies an up-regulation of AdoMetDC and vice versa, and a down-regulation of ODC implies a down-regulation of AdoMetDC and vice versa. This is formally demonstrated in Figure 22, where the expression of AdoMetDC is plotted against the expression of ODC for both epithelial and stroma cells. A least squares linear model of the double log-transformed expression levels of the enzymes as measured by initial intensity was found to yield the best statistical fit.

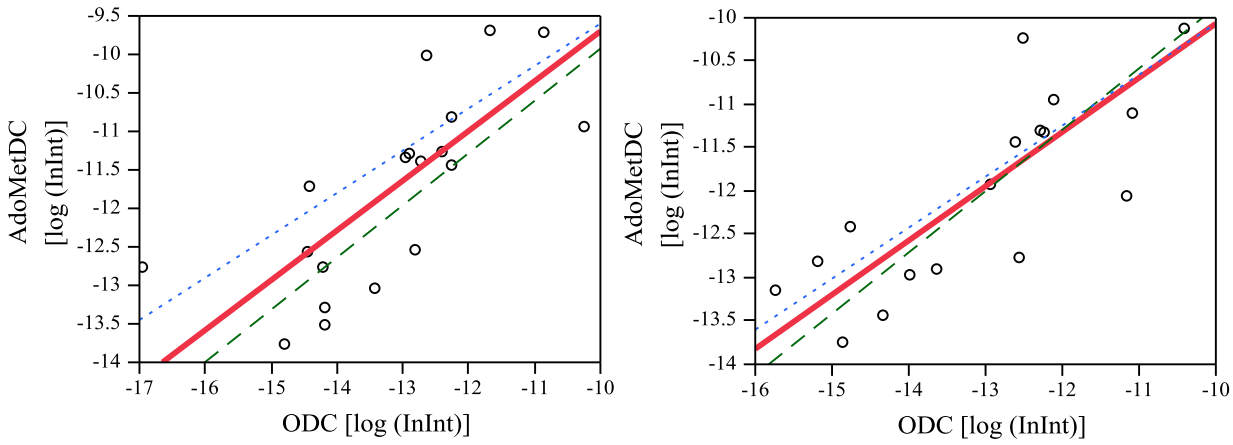

Figure 22 **Linear fit of AdoMetDC by ODC for epithelium (left) and stroma (right).** Dotted and dashed lines represent recurrent and non-recurrent subgroups, respectively.

R^2 values for epithelial and stroma tissue are listed in Table 17. Figure 22 also distinguishes between recurrent and non-recurrent cases. As demonstrated by the near-congruent fitted linear curves, however, we found no significant differences between the two experimental groups.

	Epithelium	**Stroma**
RSquare	0.5864	0.6945
RSquare Adj	0.5546	0.6709
Root Mean Square Error	0.8366	0.6672

Table 17 **Linear fit of AdoMetDC by ODC for epithelium and stroma: correlation coefficients.**

3.4.3 Correlation of catabolic enzymes

A similar phenomenon was observed for the catabolic enzyme pair. SSAT up-regulation statistically correlates with an up-regulation of OAZ. Again, a double log-transformed plot of initial intensities produced the best linear fit. Figure 23 and Table 18 document these findings.

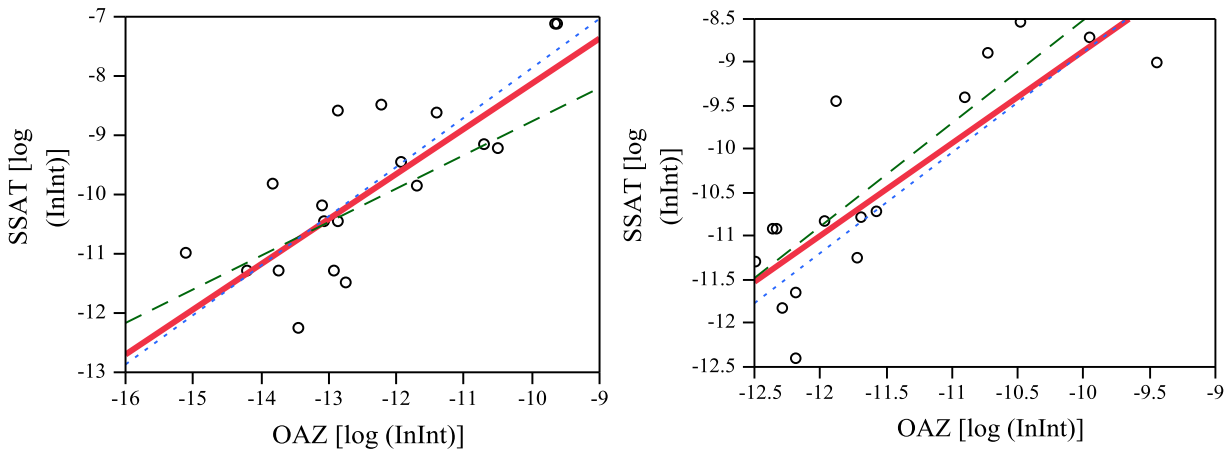

Figure 23 **Linear fit of SSAT by OAZ for epithelium (left) and stroma (right).** Dotted and dashed lines represent recurrent and non-recurrent subgroups, respectively.

As before, no significant difference was found between recurrent and non-recurrent groups and the co-regulation was observed for both epithelium and stroma. Results using the threshold/cycle-based method of quantification were comparable, if somewhat less compelling in terms of correlation coefficients.

	Epithelium	**Stroma**
RSquare	0.6024	0.6890
RSquare Adj	0.5718	0.6651
Root Mean Square Error	0.9060	0.6935

Table 18 **Linear fit of SSAT by OAZ for epithelium and stroma: correlation coefficients.**

3.4.4 Inverse correlation of SSAT and Anabolic Enzymes

Tracing the results presented in the two preceding sections 3.4.2 and 3.4.3, we found that anabolic and catabolic enzymes were similarly co-regulated, but to a lesser extent than the players previously considered. However, this co-regulation is here inverted, if we consider not the *absolute* up- or down-regulation, but the regulation *relative* to the overall expression level of the polyamine pathway. That is, as we normalize by the overall expression level (as approximated by

the mean initial intensity of the four enzymes of the pathway considered in this study) in a given sample, anabolic and catabolic enzyme regulation takes opposite directions. Where the expression of anabolic enzymes was relatively higher than the overall pathway expression level in that sample, the expression of catabolic enzymes was relatively lower than overall pathway expression, and vice versa. Figure 24 demonstrates this result plotting percentage deviation from overall pathway expression for ODC and AdoMetDC, respectively, against percentage deviation from overall pathway expression for SSAT. Both epithelium and stroma tissue types are included in the plot.

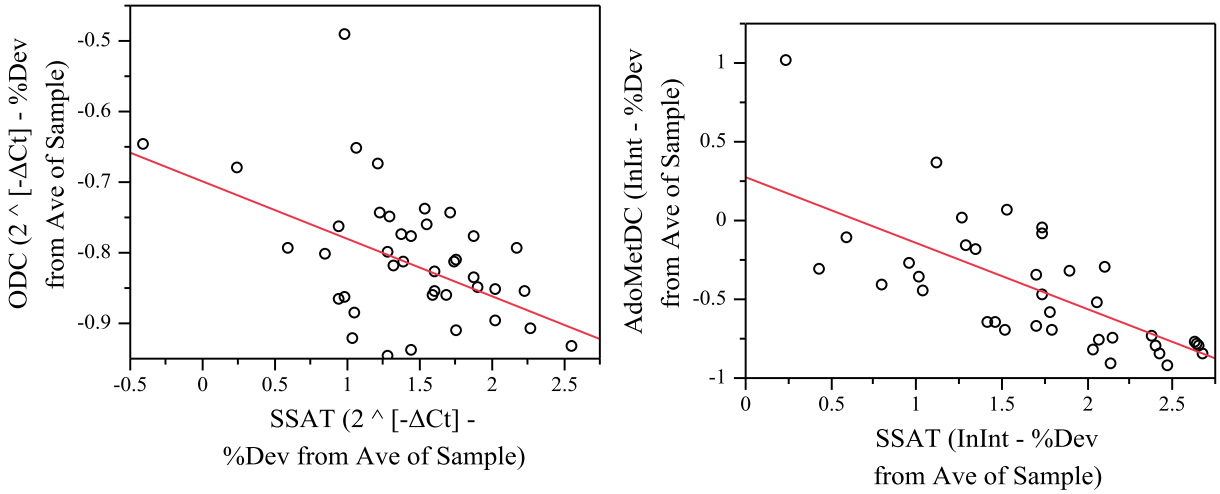

Figure 24 Linear fit of ODC (left) and AdoMetDC (right) by SSAT.

The coefficient of correlation R^2 for ODC by SSAT was 0.2213, R^2 for AdoMetDC by SSAT 0.4434. Results did not differ significantly between the initial intensity-based and the threshold/cycle-based method of quantification. Figure 24 uses $2^{-\Delta Ct}$ values for the ODC by SSAT plot (left) and initial intensity values for the AdoMetDC by SSAT plot (right).

4 Discussion

4.1 Preliminary methodological findings

The method of qPCR relies on the assumption that differences in substrate concentrations are proportional to differences in fluorescence detected. In the preliminary methodological study we put this assumption of proportionality to the test. As presented, all coefficients of correlation R^2 were satisfactorily close to 1.000 with only minimal deviations owing to unavoidable experimental error. The pilot study therefore succeeded in demonstrating the concept of qPCR and confirmed its accuracy in quantifying substrate concentrations. In addition, this preliminary trial also demonstrated the functionality of the individual primers and documented the accuracy of pipetting.

Secondly, we preliminarily tested whether the two quantification methods of qPCR deliver congruent results. The two methods are the threshold/cycle-based method on the one hand, and the initial intensity-based method on the other. As presented, the coefficients of correlation, as a measure of the goodness of fit, deviated clearly from the optimal value. Although this means that, in principle, the two quantification methods may deliver very different results, we observed no *systematic* differences. In the few cases where statistical significance depended on the quantification method chosen, this has been so noted. The sub-optimal coefficients of correlation may have been due to one or more of (a) experimental error, (b) imperfect sigmoidal curve fitting and (c) differences in amplification efficiency (178, 179).

4.2 Principal findings

This study tested two major hypotheses. Firstly, it tested the hypothesis that cases of biochemical recurrence of prostate cancer differ from cases of non-recurrence in their enzymatic profiles. In this study, enzymatic profiles were understood as the mRNA signature of cell populations. As such, the enzymatic profiles were established by quantifying mRNA. We specifically targeted the mRNA of the four biochemically most influential enzymes of the polyamine pathway. The second major hypothesis was that differences in these mRNA enzymatic profiles correspond to differences in MRS metabolomic profiles. These metabolomic profiles had been established by the use of HRMAS ^{1}H MRS, and have already been presented in a previously published study

(139). Regarding the first hypothesis, we explored two approaches, namely (a) the potential of individual enzyme expression levels to distinguish between the recurrent and non-recurrent experimental groups and (b) the potential of a combined enzymatic model to distinguish between the recurrent and non-recurrent experimental groups.

The approach examining individual enzyme expression levels found that all enzymes are expressed to a greater extent in tissue of recurrent cases than in tissue of non-recurrent cases. This difference between non-recurrent cases and cases of BCR ranged from a relative expression of 44.30% for AdoMetDC to 74.20 % for ODC. The differences in mean were observed to be statistically significant for AdoMetDC and OAZ. For ODC and SSAT, differences in mean were detected, but these differences were found to be statistically insignificant.

The approach examining the potential of a combined enzymatic model to distinguish between recurrent and non-recurrent experimental groups produced a linear combination of the four polyamine pathway enzymes here studied that can detect BCR with a significance level of $p = 0.0004$ when the expression in stroma tissue is considered and with near-significance ($p = 0.0538$) when epithelial tissue is considered.

Note, however, that it cannot fully be assessed here whether the multivariate models generated in this study can genuinely distinguish between recurrent and non-recurrent cases. Good statistical practice requires that, in a second step, the coefficients underlying the model are applied to a further testing cohort. Only if a model using those same coefficients turned out to distinguish between the previous cases and the cases of that further testing cohort, could the validity of the model be proven. As it stands, the model's validity has to be viewed as tentative and limited to the population it has been generated from.

In sum, there is nonetheless solid evidence that gene expression levels of the polyamine pathway are different in those patients that later in life develop BCR and that are more likely to be associated with metastatic progression of the disease and prostate cancer-specific mortality from those patients in whom cancer does not relapse after the procedure. All expression levels were found to be lower in non-recurrent than in recurrent cases and linear combinations of the expression levels yield a statistically striking group mean difference.

Underlying the quantification of polyamine pathway enzymes was the hypothesis that spermine, the endpoint of the pathway, may have a protective effect against PCa in general and PCa recur-

rence in particular. This hypothesis can be confirmed to an extent. It appears that, in general, the polyamine pathway is up-regulated in cases of BCR. All of ODC, AdoMetDC, SSAT and OAZ were found to be more highly expressed in this group. This observation by itself would not support the protective role of spermine: If, as we found, *anabolic* synthesis enzymes are more highly expressed in recurrent cases, too, then that most likely implies a higher level of their product, spermine, in those cases - which is the opposite of what we had reason to assume initially. When, however, we considered the correlation of enzymes among each other, we found that, relative to the general level of expression of the pathway, anabolic and catabolic enzymes are regulated inversely. This suggests that, although anabolic enzyme expression is higher in recurrent cases in absolute terms, it is lower relative to the general expression level of the pathway. The picture may be that, as has been frequently observed, pathway regulation may be cut loose in cancerous cells. Yet, while non-recurrent cases produce relatively higher levels of anabolic spermine enzymes, recurrent cases produce relatively higher cases of catabolic spermine enzymes.

A second general observation of this study is that a combined enzymatic profile distinguishes between the experimental groups much more effectively than do individual enzyme expression levels. This supports the view that cell processes are a complex integrated matter, with multiple alterations necessary to change basic metabolic variables, such as the spermine level.

A similar result was reached when testing the second major hypothesis of the study: While individual enzyme expression levels correlate only vaguely with the HRMAS ^{1}H MRS metabolomic profiles of prostate samples, combined enzymatic models give a convincing fit for many of the spectral regions. This fit was especially close for those spectral regions which can be expected to reflect the level of spermine in the tissue samples. A few best fits had correlation coefficients of $R^2 > 0.8$ and numerous spectral regions correlated with $R^2 > 0.4$.

Note, again, that the coefficients underlying the multivariate models were generated from a specific statistical population. To fully assess the general validity of the models, each model would have to be applied to a third cohort of cases that had not been part of the original population that the model has been generated from. Thus, again, caution has to be exercised when generalizing the insights of the present study to a more general population.

In sum, there is nevertheless reasonable evidence that metabolomic profiles as established by HRMAS ^{1}H MRS, a radiological method, may match enzymatic profiles as established by qPCR, a method of molecular biology. This match of profiles across two different levels of cell biology

and across two fundamentally different scientific methods is intriguing. It inspires further exploration. Limitations of the study and suggestions for a future research agenda are discussed below.

4.3 Principal findings in the context of current literature

The principal findings of this study generally fit well with the results of preceding and other current studies. With the clear qualifications discussed above, this study supports the view that spermine may act as an endogenous inhibitor of PCa (141-158). The study, as part of a wider research effort to improve the prediction of BCR pre- and postoperatively (65-68), demonstrated that predictive tools may be supplemented by enzymatic profiles. In addition, by presenting enzymatic profiles matched to metabolomic profiles, it lends molecular biological explanatory plausibility to other studies having identified MRS, i.e. a metabolome-based method, as a prognostic tool (159), in particular to those studies that identified the spermine spectral region as a potential MRS marker for BCR prediction (93).

The present study further builds on the promising results of the previously published study (139). We demonstrated that the canonical scores based on HRMAS ^{1}H MRS, which were previously shown to distinguish between BCR and non-recurrence with an accuracy of 70 to 80%, correlate with linear combinations of enzyme expression levels of the spermine pathway. While HRMAS ^{1}H MRS delivers information about the metabolomic profile of the tissue at hand, qPCR delivers information about its enzymatic profile. As enzymes are one of the prime influences on metabolite concentrations, there is clear biochemical plausibility in enzymatic and metabolomic profiles correlating.

Several differences to our initial hypothesised outcomes and to the current state of publications on the subject cannot go unmentioned, however: Firstly, while, as hypothesised, gene expression differs significantly between recurrent and non-recurrent cases, catabolic spermine enzyme expression was not uniformly up-regulated and anabolic spermine enzyme was not uniformly down-regulated in the recurrent group. Thus, the connection between BCR and the spermine pathway was not as straightforward as initially assumed. The key, as discussed above, may be the relative expression levels of the genes when compared to the overall expression level of the polyamine pathway rather than absolute expression levels. Secondly, correlation between spectral regions and polyamine pathway expression was not confined to the spermine spectral region.

This may potentially be explained by other metabolites than spermine being influenced by the polyamine pathway.

In explanation of some of the differences and to emphasise its novelty, we point out some of the unique features of the present study setting it apart from other studies: Firstly, the study is based on HRMAS ^{1}H MRS data using intact prostate specimens. The hypotheses tested here have to some extent been tested before, but the materials involved were either cell lines or aqueous solutions of the tissue components. Secondly, the current study offers a unique merging of data: (a) radiological data based on HRMAS ^{1}H MRS; (b) molecular biological data based on qPCR; and (c) histopathological data based on the pathologist's assessment. As discussed at length above, this merging of data was enabled by the fact that HRAMS ^{1}H MRS, in contrast to conventional MRS, leaves tissue samples intact for subsequent use by other methods, such as histopathological assessment and mRNA quantification.

4.4 Principal findings and clinical application

There are both diagnostic and therapeutic clinical applications of this study. The main focus of applicability of the study is, however, clearly diagnostic in nature. The recurrence of PCa, foreshadowed by rising PSA levels, is critically linked to the metastatic progression of the disease and to PCa-specific mortality. As discussed, diagnostic tools of early detection of BCR and predictive tools estimating the likelihood of BCR could support therapeutic strategy choices and enable clinicians to offer more personalized long-term PCa care after prostatectomy. Supplementing the previously published metabolomic profiles based on HRMAS ^{1}H MRS by an enzymatic profile of the polyamine pathway has been the main objective of this study. Just as the HRMAS ^{1}H MRS canonical scores presented before may be developed as predictive tools of BCR, the enzymatic profiles may be developed as such, too. A combination of both profiles, i.e. a joint score constructed from data gained by two different methods, is also imaginable. The present study is designed as proof of concept study, demonstrating that this may be possible.

Similar clinical applications are being targeted by other research groups as well. Rizzi et al., to present an example, made an effort to establish a gene signature that is potentially usable for PCa screening purposes. They also chose qPCR as the method of quantification of gene expression. All of ODC, AdoMetDC, SSAT and OAZ were part of the developed PCa gene signature – plus

four additional enzymes of the polyamine pathway. They found that PCa versus benign specimens were discriminated with 80% accuracy, 81% sensitivity and 78% specificity (180).

While that study confined itself to one method of analysis, namely qPCR, the present study combines this method with HRMAS ^{1}H MRS. And while Rizzi et al. targeted the diagnosis of PCa itself, we target the prediction of BCR after prostatectomy. Where Rizzi et al. may thus prove successful in supplementing PSA as the prime screening method, we, in the present and the preceding study, hope to establish a predictive tool where, at present, no tool is available at all.

The main diagnostic clinical application of the present study, in sum, is a tool to predict whether PCa will return after prostatectomy or not. The metabolomic, HRMAS ^{1}H MRS-based profiles of the preceding study had been a first step towards the establishment of such a tool. The enzymatic, qPCR-based profiles explored in the present study may be a second. Together they may combine to form a new paradigm in PCa treatment, as better distinction between worthwhile and futile prostatectomies may be possible and as better guidance for post-prostatectomy surveillance may be had.

In cases where recurrence is highly probable, clinicians may in the future choose not to recommend radical prostatectomy. This would spare patients such dire side effects as incontinence and impotence where no curative surgical benefit is to be had in any case. It would also save time, resources and costs for payers and providers of the health care system.

An improved prognostic tool may also guide the choice between prostatectomy and its therapeutic alternatives. Currently, High Intensity Focused Ultrasound (HIFU) and radiotherapy are perceived as two predominant radiological therapeutic alternatives (181). Radiotherapy, in turn, comprises various options, with two promising candidates being (a) brachytherapy, using radioseeds, on the one hand, and (b) external beam radiation therapy, possibly assisted by Intensity Modulated Radiation Therapy (IMRT), on the other (182, 183). Radiotherapy has also been combined with principles of hyperthermia in the usage of so called thermo-seeds (184). Further options replacing or supplementing radical prostatectomy are cryoablation, chemotherapy and hormonal therapy (185, 186). All of these options, radiological or otherwise, are currently either in use, in debate or both (181-187). An improved predictive tool for cancer recurrence would help to guide usage and resolve debate. It may assist in the choice of which single option or which combination of options is best - best for each individual patient.

Alternatively, clinicians may still recommend radical prostatectomy, but prompt (a) shorter screening intervals to detect BCR early on, and (b) more meticulous imaging modalities for the search of metastatic progression. In cases where recurrence is highly improbable, on the other hand, clinical protocols may in the future switch to a more lenient screening regime.

While such a reformed clinical paradigm is still distant, this study moves research a step closer. In an established BCR prediction protocol, specimens might be either tissue extracts from entire prostates at the time of radical prostatectomy or samples from pre-prostatectomy biopsies. The former has been the approach chosen for the present study. As it delivers information only *ex post* a given prostatectomy, however, the method would beg the question of whether that particular prostatectomy would have been necessary in the first place. That is why the latter approach, i.e. using pre-prostatectomy needle biopsy material, may prove advantageous for the next step towards clinical application. Estimating the likelihood of BCR *ex ante* prostatectomy, this method would provide clinicians with a recurrence prediction when they most need it: *Before* the surgery – a surgery that is radical, irreversible and burdened with side effects.

There are also some therapeutic implications, although application in clinical therapy is, of course, not the focus of this study. The study showed that the metabolomic and enzymatic profiles of prostate tissue differ significantly between recurrent and non-recurrent cases. The basis of this observed correlation may be a causality that can be exploited for therapy. So the first implication for therapy is that influencing the metabolome may favorably influence the course of the disease. The second implication is that influencing the enzymatic profile may favorably influence the course of the disease.

The present study therefore lends explanatory plausibility to other studies that, in some way or another, examine the effect of intervention in enzymatic and metabolomic profile on PCa and BCR. One study, to present an example, demonstrated the protective effect of the polyamine analogue N(1), N(11)-diethylnorspermine against PCa. It showed that it halts tumor growth both *in vitro* using cell lines and *in vivo* using a mouse model. Most interestingly, the study confirmed the linkage between metabolomic and enzymatic profiles: As the therapeutic polyamine analogue accumulated in the cells, enzyme counter-regulation was initiated. The study found an induction of SSAT and an inhibition of ODC (188). If such enzymatic counter-regulation could be prevented by pharmacological intervention, polyamine accumulation may increase even more and this, in turn, may help to exploit the protective effect against cancer more effectively.

This directly leads to the second therapeutic implication: Instead of (or in addition to) targeting the metabolomic profile, influencing the enzymatic profile may prove beneficial for PCa patients. One of the historically earlier attempts of intervention on the enzymatic level has been the application of ODC inhibitor alpha-difluoromethylornithine (DFMO). One study found that therapeutic intervention with DFMO against transplantable prostate adenocarcinomas in animals reduced tumor growth by 40%. A combined pharmacological regime with DFMO plus s-methylglyoxal-bisguanylhydrazone, an inhibitor of AdoMetDC, annihilated the adenocarcinomas entirely (189). Therefore, in analogy to our finding that recurrent and non-recurrent cases differ most significantly when it comes to combined enzymatic profiles (instead of when it comes to only individual enzyme levels), therapy seems most effective when it targets various enzymes at the same time.

An obstacle to therapeutic polyamine pathway intervention, however, is a series of side effects comparable to those of cytotoxic substances. When applied to human patients in clinical trials, a combined DFMO plus s-methylglyoxal-bisguanylhydrazone pharmacological regime did in fact not improve survival rates in the original study (189).

Experimental therapy approaches other than direct enzyme inhibition include the transduction of antisense polyamine pathway enzymes by means of viral vectors. Infection of prostate cancer cell lines with an adenovirus carrying antisense ODC (rAd-ODC/Ex3as) substantially inhibited tumor cell growth and arrested the cell cycle at the G1 phase (190). Note that almost all of these approaches are still in the experimental phase with cell lines and mice as the typical context of application.

Having discussed the diagnostic and therapeutic applications, it is nonetheless important to recognize that the present study is an experimental early-stage proof of concept endeavor. Its main focus has not been the clinical applicability and in so far as it is clinically applicable, the application requires further research. Implementation in medical practice is, in any case, relatively distant.

4.5 Limitations

Having discussed the principal findings of this study and their clinical applicability, several clear limitations cannot go unmentioned. The shortcomings of the study concern both the study design and the methods used. They will be discussed separately in the following.

4.5.1 Study design

Regarding the study design, the greatest shortcoming of the present study is its limited sample size. As discussed in the results section, we found statistically insignificant group mean differences for ODC and SSAT between recurrent and non-recurrent cases. We suspect that, if extrapolated to a larger sample size, these might turn statistically significant and support the findings presented here.

The second shortcoming of the present study is the fact that we have not applied the findings to a second testing cohort as yet. While we have sketched the enzymatic profile for BCR found between the BCR group and a first non-recurrent group, the profile would now have to be applied to a second matched group to test its predictive accuracy. As it stands, the present study documents a statistically significant difference between two experimental groups. To demonstrate that such a difference can be used to produce recurrence *predictions*, the profiles would have to be tested on other groups and different patient populations.

A third limitation of the design of the present study is the fact that we were not able to include all of the enzymes of the polyamine pathway. While the combined enzymatic profile clearly differed between the groups ($p = 0.0004$), it would have been intriguing to see whether a complete gene signature of the polyamine pathway might improve the distinction. This third shortcoming, however, is clearly the least worrisome: With the inclusion of ODC, AdoMetDC and SSAT we did, after all, manage to include the three rate-limiting enzymes, and thus the prime candidates of differences in pathway regulation.

4.5.2 Methods

The main methodological limitation of the present study is the choice of qPCR as a quantification method of enzyme levels. As discussed before and as utilized in this study, qPCR quantifies relative mRNA concentrations. The implicit assumption of the method is that variations in mRNA proportionally reflect upstream variations in gene expression and downstream variations in enzyme concentration and enzyme activities. None of these proportionalities is guaranteed to hold. Downstream proportionality is a particularly questionable assumption as the many mechanisms of post-translational regulation come into play.

Even if enzyme concentration were strictly proportional to mRNA expression, enzyme activities must not be. A given enzyme concentration may result in drastically different enzyme activities - depending on substrate and product feedback, antizyme control and other mechanisms of activity regulation. And even if none of these worries had any ground, there is the criticism of limited sensitivity: qPCR, among a variety of quantification methods, appears to be on the less sensitive end of the methodological spectrum (191).

Another methodological shortcoming of the present study is the limited congruence of results between the threshold/cycle-based and the initial intensity-based method of quantification. While none of the major results presented above depended on the choice of quantification method, a tighter correlation between the methods would nonetheless enhance their credibility. Both sigmoidal curve fitting, i.e. the mathematical approach underlying the initial intensity-method, and threshold/cycle-based methods have met with criticism and it is not entirely clear which, for the specific setting of this study, would be the more appropriate choice if we had to settle for only one of them (178).

The fact that the enzymatic qPCR data raised concerns intracellular enzyme levels only, while HRMAS ^{1}H MRS measurements concern both the intra- and extracellular compartments, might be considered another limitation of the study. Metabolite levels may differ significantly from enzymatic levels as metabolites exit into or enter from the extracellular compartment (166). Under these circumstances, proportionality of enzyme levels and metabolite levels cannot be guaranteed. This lack of proportionality, in turn, may explain some of the lack of correlation discussed above.

A further methodological limitation concerns the magnetic resonance side of the study, not its molecular biology portion: namely, the restriction of HRMAS ^{1}H MRS to *ex vivo* application. While ^{1}H MRS can in principle re-construct metabolomic profiles both *in vivo* and from *ex vivo* tissue samples, HRMAS ^{1}H MRS is, for the foreseeable future, available only for *ex vivo* application (81, 119, 137, 138). For the present experimental study, this was no genuine limitation, as we considered *ex vivo* specimens. As a future clinical tool, however, the effectiveness of HRMAS ^{1}H MRS metabolomic profiles would be greatly enhanced if they were available for *in vivo* application.

4.6 A research agenda

Having discussed the limitations of the study, we conclude by briefly sketching a research agenda that addresses the present limitations and offers a next step in scientific development towards improved BCR prediction. Again, improvements of study design and of methods will be discussed separately in the following.

4.6.1 Study design

A follow-up study to the present study might generally adopt the present study's design in terms of patient population, selection criteria and specimen acquisition. Most crucially, however, it would have to enlarge its sample size to reach statistically significant results where this had not been possible for the current study.

Additional cases are also needed to form a testing cohort. Once established in trials, the predictive accuracy of the enzymatic profiles could then be verified using that testing cohort. This would also yield first estimates of the enzymatic profiles' sensitivity and specificity. And it would help judge their future potential as novel diagnostic tools of BCR prediction.

Besides the enlargement of sample size, one might also consider an extension of the enzymatic spectrum. At the moment, the gene signature presented in this study is only a partial picture of the polyamine pathway. While we chose to include ODC, AdoMetDC, SSAT and OAZ, we did not quantify any of spermidine synthetase, spermine synthetase, polyamine oxidase, N-acetyl transferase or diamine oxidase. The inclusion of these enzymes might improve the predictive

accuracy of the enzymatic profile. Note, however, that we did include all the rate-limiting players of the pathway. So it is, biochemically speaking, not implausible that the inclusion of further enzymes may prove futile.

Last, a future research agenda might improve on the current study by considering non-linear models. While, in the present study, all modeling was based on least square linear regression, higher degree relations might be able to reflect more complex enzyme kinetics and metabolite interplay. As mentioned before, for example, the principal component that is the spectral region 3.29 + 3.26 ppm, yields a fit of $R^2 = 0.411$ to a combination of ODC, SSAT and OAZ when a least square linear regression is applied. Choosing a third degree polynomial function, however, the coefficient of correlation for the then non-linear model improves dramatically ($R^2 = 0.810$).

4.6.2 Methods

The most pressing methodological improvement would be the quantification of enzyme levels by means other than qPCR. As discussed, qPCR is based on mRNA quantification. Proportionality with gene expression, enzyme concentration and enzyme activity is only assumed, not guaranteed. Note however, that, since our prime interest is the establishment of a predictive tool, a lack of proportionality must not necessarily be of concern. What is needed for that purpose is a reliable fit between whatever is quantified and whatever is to be predicted. If, in the future, mRNA quantification proves expedient and the fit of mRNA with the recurrence/non-recurrence divide proves reliable, then there would be little need for methodological improvement.

This is not to say that an improved method of enzyme level quantification is unnecessary. On the contrary: Quantifying enzyme concentrations and enzyme activities directly and with certainty would grant a better understanding of the biochemical processes underlying the disease. It might also improve correlations with the metabolomic, HRMAS ^{1}H MRS-based profiles. These were, as discussed above, not entirely convincing for the individual enzymes. Part of the lack of fit might be due to the fact that it is the enzyme concentrations and their activities (not the mRNA concentrations) that influence the metabolom. In sum, a methodological improvement over the present study would be the usage of methods that directly quantify enzyme concentration and enzyme activities, not mRNA concentrations. Such methods include enzyme activity assays, and Northern and Western Blots.

A future research agenda also has to address the magnetic resonance side of the current study. Here, the limitation of HRMAS ^{1}H MRS to *ex vivo* analysis seems most pressing, as it may impede its clinical applicability. In an *ex vivo* scenario, HRMAS ^{1}H MRS could continue to be the method of analysis. This scenario would continue to rely on e.g. needle biopsy as an invasive method. One of the perceived strengths of radiological tools in clinical practice, however, is their potentially non-invasive nature. If this strength is to be exploited, the ^{1}H MRS methods here used eventually have to be transferred or transformed to work *in vivo* too.

5 Summary

In this study, we attempted to link prostate cancer recurrence to the spermine pathway. To establish and explore this link we combined a quantitative method of radiology, namely HRMAS ^{1}H MRS, with a quantitative method of molecular biology, namely qPCR. Results of the study indicate that qPCR enzymatic profiles differ significantly between recurrent and non-recurrent cases. Looking ahead, these enzymatic profiles, possibly in addition to or combination with MRS metabolomic profiles, may be developed into clinical tools predicting the likelihood of disease relapse after radical surgery. To date clinicians have virtually no tools at hand to predict the likelihood of recurrence. With the present study, we recognize the need for such predictive tools.

The study has been designed as a retrospective analysis of two cohorts of male patients (n = 16) having undergone radical prostatectomy. The average follow-up period during which the non-recurrent cohort had gone without detectable serum PSA levels was 55.8 months. The average time to the first detectable rise of serum PSA > 0.2 ng/ml after prostatectomy in the recurrent cohort was 19.9 months. Patients in the recurrent cohort were matched to patients in the non-recurrent cohort based on age, Gleason Score and clinical staging.

Biopsy tissue recovered for histopathological assessment at the time of prostatectomy served as the original specimens for the study. Specimens were subjected to histopathological assessment, HRMAS ^{1}H MRS at 14.1 T and qPCR. Using qPCR, we chose to quantify the relative mRNA concentration of the genes coding for what can be assumed to be the most influential enzymatic players of the polyamine pathway: the two rate limiting anabolic enzymes of the polyamine pathway, ornithine decarboxylase (ODC) and S-adenosyl-methionine decarboxylase (AdoMetDC); the rate-limiting catabolic enzyme, acetyl-CoA spermidine/spermine N1-acetyltransferase (SSAT); and the ODC antizyme, ornithine decarboxylase antizyme (OAZ).

We found that all of the four enzymes are expressed to a greater degree in the prostates of recurrent patients. The differences were statistically significant for the expression of AdoMetDC in epithelial cells ($p = 0.0134$) and the log-transformed expression of OAZ in epithelial cells ($p = 0.0252$). When comparing the non-recurrent to the recurrent group, relative enzyme expression was 44.30% and 56.54% for AdoMetDC and OAZ, respectively. In addition, we found that the anabolic enzymes ODC and AdoMetDC appear to be co-regulated across both cohorts ($R^2 = 0.5864$ and $R^2 = 0.6945$ for epithelial and stroma tissue, respectively). Similarly, the catabolic enzymes SSAT and OAZ correlated ($R^2 = 0.6024$ and $R^2 = 0.6890$ for epithelial and stroma tis-

sue, respectively). We also detected an inverse correlation of the expression of anabolic and catabolic enzymes relative to the general expression level of the pathway.

Combining the qPCR data with HRMAS ^{1}H MRS data, we found that singular correlations between individual enzymes and specific MRS spectral regions were, if detectable at all, weak and statistically insignificant. Using a combined model integrating several enzymes delivered more convincing results, with a top fitting correlation of $R^2 = 0.823$. We conclude that metabolomic changes appear to be best explained by complex trans-pathway changes rather than singular changes of individual enzyme expression levels.

In sum, there is solid evidence that (a) enzymatic profiles differ between recurrent and non-recurrent cases, and (b) differences in NMR spectra between recurrent and non-recurrent cases are linked to the enzymes of the spermine pathway.

The present study may be a step towards a better understanding of prostate cancer in general and BCR in particular. With further development still to come, enzymatic profiles, in addition to or in combination with HRMAS ^{1}H MRS metabolomic profiles, may be developed into clinical tools. As clinical tools, the profiles may be applied to help (a) better judge the benefits of radical surgery, a procedure that often comes with drastic side effects, (b) weigh its benefits against alternative treatment options, and (c) adjust post-surgery monitoring regimes according to whether recurrence is probable or not. While we recognize the limitations of the present study, it demonstrates the potential of qPCR-based enzymatic profiles and of HRMAS ^{1}H MRS-based metabolomic profiles. And while this study is experimental and explorative in nature, it may encourage further research.

Zusammenfassung

HINTERGRUND Die Studie untersucht den postulierten Zusammenhang zwischen Spermin-Stoffwechsel und Prostatakarzinom. Sie versucht, diesen für die Vorhersage von Rezidiven nutzbar zu machen. Dazu kombiniert sie Histopathologie, High Resolution Magic Angle Spinning ^{1}H-Magnetresonanzspektroskopie (HRMAS ^{1}H MRS) und quantitative Polymerase-Kettenreaktion (qPCR).

METHODIK Die Studie betrachtet retrospektiv eine Kohorte männlicher Patienten mit Prostatakarzinom (n = 16) im Zeitraum (19,9 Monate) zwischen radikaler Prostatektomie und biochemischem Rezidiv (PSA > 0,2 ng/ml). Die Kontrollkohorte setzt sich aus randomisiert ausgewählten und per Matching (Alter, Gleason-Score, klinisches Stadium) zugewiesenen Patienten mit Prostatakarzinom zusammen, bei denen im Beobachtungszeitraum (55,8 Monate nach Prostatektomie) kein PSA-Rezidiv nachweisbar war. Untersuchungsmaterial sind zum Zeitpunkt der Prostatektomie gewonnene Biopsat-Serien. Es erfolgte (1) eine histopathologische Bewertung, (2) die Aufzeichnung und quantitative Auswertung von Magnetresonanzspektren per HRMAS ^{1}H MRS (14 Tesla), (3) die mRNA-Quantifizierung der Genexpression von Schrittmacherenzymen im Polyaminstoffwechsel per qPCR.

ERGEBNISSE Die Expression der für AdoMetDC ($p = 0{,}0134$) und OAZ ($p = 0{,}0252$) kodierenden Gene unterscheidet sich in der Rezidiv-Kohorte signifikant von derjenigen in der Kontrollkohorte. Die anabolen Enzyme ODC und AdoMetDC korrelieren dabei miteinander, sowohl in Epithel ($R^2 = 0{,}5864$) als auch Stroma ($R^2 = 0{,}6945$). Gleiches gilt für die katabolen Enzyme SSAT ($R^2 = 0{,}6024$) und OAZ ($R^2 = 0{,}6890$). In multivariaten Analysen korrelieren diese Genexpressionsmuster mit der Intensität bestimmter Regionen des NMR-Spektrums der Proben. Während für individuelle Enzyme kein signifikanter Vorhersagewert nachgewiesen werden kann, erreichen kombinierte lineare Modelle (Methode der kleinsten Fehlerquadrate) in den betrachteten Kohorten Korrelationskoeffizienten von bis zu $R^2 = 0{,}823$.

DISKUSSION Die Studie legt nahe, dass sich die Genexpressionsmuster von Rezidiv-Patienten bereits bei Prostatektomie signifikant von denjenigen der Patienten ohne späteres Rezidiv unterscheiden. Unterschiede der Genexpressionsmuster korrelieren zudem mit Unterschieden im Magnetresonanzspektrum der Gewebe. Perspektivisch könnte das helfen, die Rezidivwahrscheinlichkeit von Prostatakarzinomen besser einzuschätzen und das klinische Monitoring fallgemäß anzupassen.

List of Abbreviations

%Dev	Percentage deviation
[c]	Concentration
µl	Microliters
µm	Micrometers
^{1}H MRS	Proton Magnetic Resonance Spectroscopy
5MTA	5-methylthioadenosine
AdoMetDC	S-adenosyl-methionine decarboxylase
AE	Amplification efficiency
AJCC	American Joint Commission on Cancer
AUC	Area und the curve
Ave	Average
BCR	Biochemical recurrence
BPH	Benign prostatic hyperplasia
C	Cycle
Ca	Cancer
cDNA	Complementary DNA
c-MYC	Cellular myelocytomatosis oncogene
CPMG	Carr-Purcell-Meiboom-Gill
Ct	Cycle at threshold t
D_2O	Deuterium oxide
DAO	Diamine oxidase
Dev	Deviation
DF	Degrees of freedom
DNA	Desoxyribonucleic acid
DNTP	Desoxynucleosid triphosphate
DTT	Dithiothreitol
EtOH	Ethanol
GS	Gleason Score
HE	Hematoxylin eosin
HPLC	High pressure liquid chromatography
HRMAS	High Resolution Magic Angle Spinning

Hz	Hertz
InInt	Initial intensity
kHz	Kilohertz
LCM	Laser capturing microdissection
MHz	Megahertz
MRI	Magnetic Resonance Imaging
mRNA	Messenger RNA
MRS	Magnetic Resonance Spectroscopy
MRS Int	Magnetic resonance spectroscopy intensity
Msec	milliseconds
MW	Megawatt
Ng	Nanograms
NMR	Nuclear magnetic resonance
OAZ	Ornithine decarboxylase antizyme
ODC	Ornithine decarboxylase
PAO	Polyamine oxidase
PCa	Prostate cancer
PCR	Polymerase chain reaction
Ppm	Parts per million
PSA	Prostate-specific antigen
qPCR	Quantitative real time PCR
RNA	Ribonucleic acid
ROC	Receiver operating characteristic
rRNA	ribosomal RNA
SAM	S-adenosyl-methionine
SAMHC	S-adenosyl-S-methyl homocysteamine
Spm	Spermine
SSAT	Acetyl-CoA spermidine/spermine N1-acetyl-transferase
StDev	Standard deviation
T	Tesla
TNM	Tumor, node, metastasis
Vs	Versus
x ^ y	x^y

List of Figures

Figure 1 Results from a preceding study. The study identified 27 spectral regions, constructing a canonical score from selected principal components as the metabolomic profile of prostate cancer recurrence. The canonical score differentiates between cases of biochemical recurrence (BCR) and cases without recurrence of PCa (match) with statistical significance. The left two plots use the four and the right two plots the nine statistically most influential principal components. The upper two plots compare the recurrent group with a non-recurrent group matched by clinical staging. The lower two plots apply the score to a second non-recurrent group matched by pathological staging (139). 13

Figure 2 Magnetic resonance spectrum of benign and malignant prostate tissue. The spermine peak in the metabolomic profile differs between benign (A) and cancerous tissue (B). The spectra stem from HRMAS ^{1}H MRS at 9.4 T (400 MHz) (160). 15

Figure 3 Correlation between spermine concentration and volume percentage of benign epithelium. The figure reproduces the key chart of the preceding study demonstrating that spermine concentrations as measured by MRS and volume percentage of benign epithelium as measured by quantitative histopathology correlate (160)..... 15

Figure 4 The polyamine pathway. Spermine is produced from ornithine in a sequence of steps with putrescine and spermidine as metabolic predecessors and a total of eight different enzymes directly catalyzing the process (161). Names of the enzymes 1 to 8 are given in Table 1. 5MTA: 5-methylthioadenosine; SAM: S-adenosyl-methionine; SAMHC: S-adenosyl-S-methyl homocysteamine. 16

Figure 5 Tissue samples after HE-staining. Displayed are two samples of prostate tissue exhibiting predominantly malignant growth patterns, featuring one highly proliferative exhibit (left) and one moderately proliferative exhibit (right). Pictures were taken using an Olympus BX41 Microscope and Imaging System at a ten-fold magnification. 26

Figure 6 Scheme of positive controls. Each of the steps of qPCR, starting from the original tissue sample to the actual amplification process, was accompanied by a newly entering positive control. The top line portrays the procedural steps the samples underwent. The bottom three lines portray the steps each of the three positive controls underwent. Positive controls were produced either from commercially available mRNA of human prostate tissue (for the extraction and synthesis steps) or from a previously accumulated stock of cDNA (for the amplification step). 34

Figure 7 Amplification efficiency versus cycle by enzyme. Ct values are for a common randomly chosen threshold of the log-linear phase. The amplification efficiency routinely differs from its optimal assumed value

of 2.00. The plot indicates that variation occurs both across enzymes and with entry cycle. The two variants A and B of 18s represent data from two separate qPCR runs. 35

Figure 8 Accuracy control tool. The tool analyses the experimental accuracy by calculating the absolute span between minimum and maximum values of technical multiples and their standard deviations at a given threshold. If certain accuracy limits are exceeded, the tool points out which samples should be re-run. 36

Figure 9 Example of a qPCR quantification plot. Fluorescence is plotted against cycle number. Each curve represents the amplification process of one well, i.e. of one gene in one sample. The two curves on the left are technical duplicates of the housekeeping gene (here: 18s mRNA). The three curves on the right are technical triplicates of the gene of interest (here: OAZ). 37

Figure 10 Schematic qPCR quantification plot. 38

Figure 11 Linear fit of Ct and concentration (log-transformed) by protein. 45

Figure 12 Bivariate fit of ΔCt by initial intensity (log-transformed) for ODC (left) and AdoMetDC (right). 47

Figure 13 ODC by recurrent vs non-recurrent. Left: $2^{-\Delta Ct}$ (matched pairs); right: initial intensity. 48

Figure 14 AdoMetDC by recurrent vs non-recurrent. Left: $2^{-\Delta Ct}$ (matched pairs); right: initial intensity. 49

Figure 15 SSAT by recurrent vs non-recurrent. Left: $2^{-\Delta Ct}$ (matched pairs); right: initial intensity. 50

Figure 16 OAZ by recurrent vs non-recurrent. Left: $2^{-\Delta Ct}$ (matched pairs); right: initial intensity. 51

Figure 17 Linear fit of MRS intensity to ODC level: Two selected examples. 53

Figure 18 Linear fit of MRS intensity to AdoMetDC level: Two selected examples. 53

Figure 19 Linear fit of MRS intensity to SSAT level: Two selected examples 54

Figure 20 Linear fit of MRS intensity to OAZ level: Two selected examples 55

Figure 21 C-Myc by recurrent vs non-recurrent. Left: $2^{-\Delta Ct}$ (matched pairs); right: initial intensity. 57

Figure 22 Linear fit of AdoMetDC by ODC for epithelium (left) and stroma (right). Dotted and dashed lines represent recurrent and non-recurrent subgroups respectively. 58

Figure 23 Linear fit of SSAT by OAZ for epithelium (left) and stroma (right). Dotted and dashed lines represent recurrent and non-recurrent subgroups respectively. 59

Figure 24 Linear fit of ODC (left) and AdoMetDC (right) by SSAT. 60

List of Tables

Table 1 Enzymes of the polyamine pathway. Numbers refer to Figure 4. There are three rate-limiting enzymes involved in the pathway. Ornithine decarboxylase (ODC) and S-adenosyl-methionine decarboxylase (AdoMetDC) are the rate limiting anabolic enzymes, while acetyl-CoA spermidine/spermine N1-acetyl-transferase (SSAT) is the rate limiting catabolic enzyme. 17

Table 2 Proteins chosen for quantification and their physiological functions. 19

Table 3 Clinical characteristics of patient population. The column 'age' lists the respective age at time of prostatectomy. The column 'period' lists the time gap between prostatectomy and first PSA increase for the recurrent group, and the total observation period after prostatectomy for the non-recurrent group, during which no PSA increase has been detected after prostatectomy. 23

Table 4 Clinical characteristics of patient sub-population. 50% of the main population from the preceding MRS study were selected to supplement MRS data with enzymatic data for this sub-population. The column 'age' lists the respective age at time of prostatectomy. The column 'period' lists the time gap between prostatectomy and first PSA increase for the recurrent group, and the total observation period after prostatectomy for the non-recurrent group, during which no PSA increase has been detected after prostatectomy. 24

Table 5 Hematoxylin–eosin staining protocol. Staining protocol used for the histopathological assessment. 25

Table 6 HE quick staining protocol. Protocol used before laser capturing microdissection. 30

Table 7 Reagents used in RNA extraction and cDNA synthesis. 31

Table 8 Cycling protocol. Protocol used for qPCR amplification on an *ABI PRISM 7000 Fast LightCycler*. 32

Table 9 Primers used in qPCR. All primers were ordered from *SABiosciences* (USA). 32

Table 10 Linear fit of Ct and concentration (log-transformed) by protein: R^2 square values. 46

Table 11 ΔCt by initial intensity (log-transformed): Bivariate fit for ODC (left) and AdoMetDC (right) 47

Table 12 ODC by recurrent vs non-recurrent: Analysis of variance 48

Table 13 ODC by recurrent vs non-recurrent: Wilcoxon / Kruskal-Wallis Tests (Rank Sums) 49

Table 14 Recurrent vs non-recurrent - combined enzyme model: Whole model test (using log-transformed initial intensity). 51

Table 15 Recurrent vs non-recurrent - combined enzyme model: Effect likelihood ratio tests (using log-transformed initial intensity). 52

Table 16 Linear fit of MRS intensity to enzymatic profile: Top nine correlations found 56

Table 17 Linear fit of AdoMetDC by ODC for epithelium and stroma: correlation coefficients. 58

Table 18 Linear fit of SSAT by OAZ for epithelium and stroma: correlation coefficients. 59

Bibliography

1 Jemal A, Siegel R, Ward E, et al. Cancer statistics, 2008. CA Cancer J Clin 2008;58:71-96.

2 Rohde V, Wasem J, Katalinic A. Gesundheitsberichterstattung des Bundes - Prostataerkrankungen. In. Berlin: Robert Koch Institut in Kooperation mit dem Statistischen Bundesamt; 2007:1-27.

3 Jemal A, Murray T, Ward E, et al. Cancer statistics, 2005. CA Cancer J Clin 2005;55:10-30.

4 Jemal A, Thomas A, Murray T, Thun M. Cancer statistics, 2002. CA Cancer J Clin 2002;52:23-47.

5 Bertz J, Dahm S, Jörg Haberland, Kraywinkel K, Kurth B-M, Wolf U. Verbreitung von Krebserkrankungen in Deutschland. Entwicklung der Prävalenzen zwischen 1990 und 2010. In: RKI, ed. Beiträge zur Gesundheitsberichterstattung des Bundes. Berlin: Robert-Koch-Institut; 2010.

6 Hankey B, Feuer E, Clegg L, et al. Cancer surveillance series: interpreting trends in prostate cancer—part I: Evidence of the effects of screening in recent prostate cancer incidence, mortality, and survival rates. J Natl Cancer Inst 1999;91:1017–24.

7 Stephenson AJ, Kattan MW, Eastham JA, et al. Prostate Cancer–Specific Mortality After Radical Prostatectomy for Patients Treated in the Prostate-Specific Antigen Era. J Clin Oncol 2009;27:4300-5.

8 Stephenson AJ, Kattan MW, Eastham JA, et al. Defining Biochemical Recurrence of Prostate Cancer After Radical Prostatectomy: A Proposal for a Standardized Definition. J Clinical Oncol 2006;24:3973-8.

9 Eisenberger M, Partin A, Pound C. Natural history of progression of patients with biochemical (PSA) relapse following radical prostatectomy: Update. Proc Am Soc Clin Oncol 2003;22:380.

10 Pound CR, Partin AW, Eisenberger MA, Chan DW, Pearson JD, Walsh PC. Natural history of progression after PSA elevation following radical prostatectomy. JAMA 1999;281:1591-7.

11 Freedland S, Humphreys E, Mangold L. Risk of prostate cancer-specific mortality following biochemical recurrence after radical prostatectomy. JAMA 2005;294:433-9.

12 Maximum androgen blockade in advanced prostate cancer: An overview of the randomised trials— Prostate Cancer Trialists' Collaborative Group. Lancet 2000;355:1491-8.

13 D'Amico A, Moul J, Carroll P. Surrogate end point for prostate cancer-specific mortality after radical prostatectomy or radiation therapy. J Natl Cancer Inst 2003;95:1376-83.

14 Bianco FJ, Scardino P, Eastham J. Radical prostatectomy: Long-term cancer control and recovery of sexual and urinary function ("trifecta"). Urology 2005;66:83-94.

15 Zhou P, Chen M, McLeod D. Predictors of prostate cancer-specific mortality after radical prostatectomy or radiation therapy. J Clin Oncol 2005;23:6992-8.

16 Amling C, Bergstralh E, Blute M. Defining prostate specific antigen progression after radical prostatectomy: What is the most appropriate cut point? J Urol 2001;165:1146-51.

17 Gretzer M, Trock B, Han M. A critical analysis of the interpretation of biochemical failure in surgically treated patients using the American Society for Therapeutic Radiation and Oncology criteria. J Urol 2002;168.

18 Kuban D, Thames H, Shipley W. Defining recurrence after radiation for prostate cancer. J Urol 2005;173:1871-8.

19 Scher H, Eisenberger M, D'Amico A. Eligibility and outcomes reporting guidelines for clinical trials for patients in the state of a rising prostatespecific antigen: Recommendations from the Prostate- Specific Antigen Working Group. J Clin Oncol 2004;22.

20 Carroll P, Lee K, Fuks Z, Kantoff P. Cancer of the Prostate. In: DeVita V, Hellman S, Rosenberg S, eds. Cancer: Principle and Practice of Oncology. 6th ed. Philadelphia: Lippincott Williams & Wilkins; 2001.

21 Gaudin PB, Epstein JI. Adenosis of the prostate. Histologic features in needle biopsy specimens. Am J Surg Pathol 1995;19:737-47.

22 Andriole G, Crawford E, Grubb RI, et al. Mortality results from a randomized prostate-cancer screening trial. N Engl J Med 2009;360:1310–9.

23 Schroder F, Hugosson J, Roobol M, et al. Screening and prostate-cancer mortality in a randomized European study. N Engl J Med 2009;360:1320–8.

24 Gleason D. Classification of prostatic carcinomas. Cancer Chemother Rep 1966;50:125.

25 Broders A. Epithelium of the genito-urinary organs. Ann Surg 1922;75:574.

26 Mostofi F, Davis C, Sesterhenn I. Pathology of carcinoma of the prostate. Cancer 1992;70:235.

27 Gaeta J, Asiwartham J, Miller G. Histologic grading of primary prostate cancer: a new approach to an old problem. J Urol 1980;123:689.

28 Bocking A, Kiehn J, Heinzel-Wach M. Combined histologic grading of prostatic carcinoma. Cancer 1982;50:288.

29 Brawn P, Ayala A, von Eschenbach A. Histological grading of prostate adenocarcinoma: the development of a new system and comparison with other methods. Cancer 1982;49:525.

30 Cotran R, Kumar V, Robbins S. Pathologic basis of disease. 5th ed. Philadelphia: W.B. Saunders; 1994.

31 Shariat S, Karakiewicz P, Margulis V, Kattan M. Inventory of prostate cancer predictive tools. Curr Opin Urol 2008;18:279–96.

32 Shariat S, Karakiewicz P, Suardi N, Kattan M. Comparison of nomograms with other methods for predicting outcomes in prostate cancer: A critical analysis of the literature. Clin Cancer Res 2008;14:4400–7.

33 Gleason D. Histologic grading of prostate cancer: a perspective. Hum Pathol 1992;23:273.

34 Oesterling J, Fuks Z, Lee C, Scher H. Cancer of the prostate. In: DeVita V, Jr, Hellman S, Rosenberg S, eds. Cancer Principles & Practice of Oncology. Philadelphia: Lippincott-Raven; 1997:1322-86.

35 Lilja H, Ulmert D, Vickers A. Prostate-specific antigen and prostate cancer: Prediction, detection and monitoring. Nat Rev Cancer 2008;8:268–78.

36 Brawley OW, Barnes S, Parnes H. The future of prostate cancer prevention. Ann N Y Acad Sci 2001;952:145-52.

37 Nelson KA, Witte JS. Androgen receptor CAG repeats and prostate cancer. Am J Epidemiol 2002;155:883-90.

38 Putzi MJ, De Marzo AM. Prostate pathology: histologic and molecular perspectives. Hematol Oncol Clin North Am 2001;15:407-21.

39 Still K, Robson CN, Autzen P, Robinson MC, Hamdy FC. Localization and quantification of mRNA for matrix metalloproteinase-2 (MMP-2) and tissue inhibitor of matrix metalloproteinase-2 (TIMP-2) in human benign and malignant prostatic tissue. Prostate 2000;42:18-25.

40 Signoretti S, Waltregny D, Dilks J, et al. p63 is a prostate basal cell marker and is required for prostate development. Am J Pathol 2000;157:1769-75.

41 Cohen RJ, Holland JW, Redmond SL, McNeal JE, Dawkins HJ. Identification of the glycosaminoglycan keratan sulfate in the prostatic secretory cell. Prostate 2000;44:204-9.

42 Dawkins HJ, Sellner LN, Turbett GR, et al. Distinction between intraductal carcinoma of the prostate (IDC-P), high-grade dysplasia (PIN), and invasive prostatic adenocarcinoma, using molecular markers of cancer progression. Prostate 2000;44:265-70.

43 Recker F, Kwiatkowski MK, Piironen T, et al. Human glandular kallikrein as a tool to improve discrimination of poorly differentiated and non-organ-confined prostate cancer compared with prostate-specific antigen. Urology 2000;55:481-5.

44 Liu AY, True LD, LaTray L, et al. Cell-cell interaction in prostate gene regulation and cytodifferentiation. Proc Natl Acad Sci U S A 1997;94:10705-10.

45 Liu AY, LaTray L, van Den Engh G. Changes in cell surface molecules associated with in vitro culture of prostatic stromal cells. Prostate 2000;44:303-12.

46 Elsasser-Beile U, Przytulski B, Gierschner D, et al. Comparison of the activation status of tumor infiltrating and peripheral lymphocytes of patients with adenocarcinomas and benign hyperplasia of the prostate. Prostate 2000;45:1-7.

47 Fry PM, Hudson DL, O'Hare MJ, Masters JR. Comparison of marker protein expression in benign prostatic hyperplasia in vivo and in vitro. BJU Int 2000;85:504-13.

48 Liu AY. Differential expression of cell surface molecules in prostate cancer cells. Cancer Res 2000;60:3429-34.

49 Ghossein RA, Bhattacharya S. Molecular detection and characterisation of circulating tumour cells and micrometastases in solid tumours. Eur J Cancer 2000;36:1681-94.

50 Belair CD, Yeager TR, Lopez PM, Reznikoff CA. Telomerase activity: a biomarker of cell proliferation, not malignant transformation. Proc Natl Acad Sci U S A 1997;94:13677-82.

51 Ransohoff DF, McNaughton Collins M, Fowler FJ. Why is prostate cancer screening so common when the evidence is so uncertain? A system without negative feedback. Am J Med 2002;113:663-7.

52 Partin A, Kattan M, Subong E, et al. Combination of prostate-specific antigen, clinical stage, and Gleason score to predict pathological stage of localized prostate cancer. A multi-institutional update [see comments]. JAMA 1997;277:1445-51.

53 Ohori M, Kattan MW, Koh H, et al. Predicting the presence and side of extracapsular extension: a nomogram for staging prostate cancer. J Urol 2004;171:1844-9; discussion 9.

54 Kattan MW, Eastham JA, Wheeler TM, et al. Counseling men with prostate cancer: a nomogram for predicting the presence of small, moderately differentiated, confined tumors. J Urol 2003;170:1792-7.

55 Horiguchi A, Nakashima J, Horiguchi Y, et al. Prediction of extraprostatic cancer by prostate specific antigen density, endorectal MRI, and biopsy Gleason score in clinically localized prostate cancer. Prostate 2003;56:23-9.

56 Naya Y, Ochiai A, Troncoso P, Babaian RJ. A comparison of extended biopsy and sextant biopsy schemes for predicting the pathological stage of prostate cancer. J Urol 2004;171:2203-8.

57 Woolf SH. The accuracy and effectiveness of routine population screening with mammography, prostate-specific antigen, and prenatal ultrasound: a review of published scientific evidence. Int J Technol Assess Health Care 2001;17:275-304.

58 Bunting PS. Screening for prostate cancer with prostate-specific antigen: beware the biases. Clin Chim Acta 2002;315:71-97.

59 Guinan P, Bhatti R, Ray P. An evaluation of prostate specific antigen in prostatic cancer. J Urol 1987;137:686-9.

60 Xu J, Stolk JA, Zhang X, et al. Identification of differentially expressed genes in human prostate cancer using subtraction and microarray. Cancer Res 2000;60:1677-82.

61 Jiang Z, Woda BA, Rock KL, et al. P504S: a new molecular marker for the detection of prostate carcinoma. Am J Surg Pathol 2001;25:1397-404.

62 Yang XJ, Wu CL, Woda BA, et al. Expression of alpha-Methylacyl-CoA racemase (P504S) in atypical adenomatous hyperplasia of the prostate. Am J Surg Pathol 2002;26:921-5.

63 Jiang Z, Wu CL, Woda BA, et al. P504S/alpha-methylacyl-CoA racemase: a useful marker for diagnosis of small foci of prostatic carcinoma on needle biopsy. Am J Surg Pathol 2002;26:1169-74.

64 Beach R, Gown AM, De Peralta-Venturina MN, et al. P504S immunohistochemical detection in 405 prostatic specimens including 376 18-gauge needle biopsies. Am J Surg Pathol 2002;26:1588-96.

65 Karakiewicz P, Hutterer G. Predictive models and prostate cancer. Nat Clin Pract Urol 2008;5:82–92.

66 Shariat S, Walz J, Roehrborn C, et al. External validation of a biomarkerbased preoperative nomogram predicts biochemical recurrence after radical prostatectomy. J Clin Oncol 2008;26:1526-31.

67 Steuber T, O'Brien M, Lilja H. Serum markers for prostate cancer: A rational approach to the literature. Eur Urol 2008;54:31–40.

68 Makarov D, Trock B, Humphreys E, et al. Updated nomogram to predict pathologic stage of prostate cancer given prostate-specific antigen level, clinical stage, and biopsy Gleason score (Partin tables) based on cases from 2000 to 2005. Urology 2007;69:1095–101.

69 Hara R, Jo Y, Fujii T, et al. Optimal approach for prostate cancer detection as initial biopsy: Prospective randomized study comparing transperineal versus transrectal systematic 12-core biopsy. Urology 2008;71:191–5.

70 Wright J, Lange P. Newer potential biomarkers in prostate cancer. Rev Urol 2007;9:207–13.

71 Urenjak J, Williams S, Gadian D, Noble M. Proton nuclear magnetic resonance spectroscopy unambiguously identifies different neural cell types. J Neurosci 1993;13:981-9.

72 Mountford C, Doran S, Lean C, Russell P. Cancer pathology in the year 2000. Biophys Chem 1997;68:127-35.

73 Mountford C, Lean C, Hancock R, et al. Magnetic resonance spectroscopy detects cancer in draining lymph nodes. Invasion & Metastasis 1993;13:57-71.

74 Jordan K, Cheng L. NMR-based metabolomics approach to target biomarkers for human prostate cancer. Future Drugs 2007;4:389-400.

75 Qiuhong H, Xu RZ, Shkarin P, et al. Magnetic resonance spectroscopic imaging of tumor metabolic markers for cancer diagnosis, metabolic phenotyping, and characterization of tumor microenvironment. Disease Markers 2003;19:69-94.

76 Wieruszeski JM, Bohin A, Bohin JP, Lippens G. In vivo detection of the cyclic osmo-regulated periplasmic glucan of Ralstonia solanacearum by high-resolution magic angle spinning NMR. J Magn Reson 2001;151:118-23.

77 Heerschap A, Jager G, van der Graaf M, et al. In vivo proton MR spectroscopy reveals altered metabolite content in malignant prostate tissue. Anticancer Res 1997;17:1455-60.

78 Taylor JL, Wu CL, Cory D, Gonzalez RG, Bielecki A, Cheng LL. High-resolution magic angle spinning proton NMR analysis of human prostate tissue with slow spinning rates. Magn Reson Med 2003;50:627-32.

79 Cheng L, Pohl U. The role of NMR-based metabolomics in cancer. In: Lindon J, Nicholls J, Holmes E, eds. The handbook of metabonomics and metabolomics. Amsterdam: Elsevier; 2007:345–74.

80 Straubinger K, Schick F, Lutz O. Influence of pulse angle variations on stimulated echo acquisition mode proton nuclear magnetic resonance spectra of AB spin systems: theory and experiments with citrate. Magnetic Resonance Materials in Physics, Biology and Medicine 1998;7:88-94.

81 Cox I. Development and applications of in vivo clinical magnetic resonance spectroscopy. Prog Biophys Mol Biol 1996;65:45-81.

82 Wiechert W, de Graaf A. In vivo stationary flux analysis by 13C labeling experiments. Adv Biochem Eng Biotechnol 1996; 54:109-54.

83 Parivar F, Hricak H, Shinohara K, et al. Detection of locally recurrent prostate cancer after cryosurgery: evaluation by transrectal ultrasound, magnetic resonance imaging, and three-dimensional proton magnetic resonance spectroscopy. Urology 1996;48:594-9.

84 Kurhanewicz J, Vigneron D, Hricak H, et al. Prostate cancer: metabolic response to cryosurgery as detected with 3D H-1 MR spectroscopic imaging. Radiology 1996;200:489-96.

85 Heerschap A, Jager G, van der Graaf M, Barentsz J, Ruijs S. Proton MR spectroscopy of the normal human prostate with an endorectal coil and a double spin-echo pulse sequence. Magn Reson Med 1997;37:204-13.

86 Van der Graaf M, van den Boogert H, Jager G, Barentsz J, Heerschap A. Human prostate: Multisection proton MR spectroscopic imaging with a single spin-echo sequence--preliminary experience. Radiology 1999;213:919-25.

87 Costello L, Franklin R, Narayan P. Citrate in the diagnosis of prostate cancer. Prostate 1999;38:237-45.

88 Swanson MG, Vigneron DB, Tran TK, Sailasuta N, Hurd RE, Kurhanewicz J. Single-voxel oversampled J-resolved spectroscopy of in vivo human prostate tissue. Magn Reson Med 2001;45:973-80.

89 Adusumilli S, Pretorius ES. Magnetic resonance imaging of prostate cancer. Semin Urol Oncol 2002;20:192-210.

90 Yu KK, Scheidler J, Hricak H, et al. Prostate cancer: prediction of extracapsular extension with endorectal MR imaging and three-dimensional proton MR spectroscopic imaging. Radiology 1999;213:481-8.

91 Kurhanewicz J, Swanson MG, Wood PJ, Vigneron DB. Magnetic resonance imaging and spectroscopic imaging: Improved patient selection and potential for metabolic intermediate endpoints in prostate cancer chemoprevention trials. Urology 2001;57:124-8.

92 Lynch M, Masters J, Pryor J, et al. Ultra high field NMR spectroscopic studies on human seminal fluid, seminal vesicle and prostatic secretions. J Pharm Biomed Anal 1994;12:5-19.

93 Lynch M, Nicholson J. Proton MRS of human prostatic fluid: correlations between citrate, spermine, and myo-inositol levels and changes with disease. Prostate 1997;30:248-55.

94 Willker W, Flogel U, Leibfritz D. A 1H/13C inverse 2D method for the analysis of the polyamines putrescine, spermidine ans spermine in cell extracts and biofluids. NMR Biomed 1998;11:47-54.

95 Hahn P, Smith I, Leboldus L, Littman C, Somorjai R, Bezabeh T. The classification of benign and malignant human prostate tissue by multivariate analysis of 1H magnetic resonance spectra. Cancer Res 1997;57:3398-401.

96 van der Graaf M, Schipper RG, Oosterhof GO, Schalken JA, Verhofstad AA, Heerschap A. Proton MR spectroscopy of prostatic tissue focused on the detection of spermine, a possible biomarker of malignant behavior in prostate cancer. Magma 2000;10:153-9.

97 Cornel E, Smits G, Oosterhof G, et al. Characterization of human prostate cancer, benign prostatic hyperplasia and normal prostate by in vitro 1H and 31P magnetic resonance spectroscopy. J Urol 1993;150:2019-24.

98 Kurhanewicz J, Dahiya R, Macdonald J, Chang L, James T, Narayan P. Citrate alterations in primary and metastatic human prostatic adenocarcinomas: 1H magnetic resonance spectroscopy and biochemical study. Magn Reson Med 1993;29:149-57.

99 Fowler A, Pappas A, Holder J, et al. Differentiation of human prostate cancer from benign hypertrophy by in vitro 1H NMR. Magn Reson Med 1992;25:140-7.

100 Schiebler M, Miyamoto K, White M, Maygarden S, Mohler J. In vitro high resolution 1H-spectroscopy of the human prostate: benign prostatic hyperplasia, normal peripheral zone and adenocarcinoma. Magn Reson Med 1993;29:285-91.

101 Cornel E, Smits G, de Ruijter J, et al. In vitro proton magnetic resonance spectroscopy of four human prostate cancer cell lines. Prostate 1995;26:275-80.

102 Cheng LL, Chang IW, Louis DN, Gonzalez RG. Correlation of high-resolution magic angle spinning proton magnetic resonance spectroscopy with histopathology of intact human brain tumor specimens. Cancer Res 1998;58:1825-32.

103 Chapman D, Oldfield E, Doskocilová D, Schneider B. NMR of gel and liquid crystalline phospholipids spinning at the "magic angle". FEBS Letters 1972;25:261-4.

104 Cheng LL, Anthony DC, Comite AR, Black PM, Tzika AA, Gonzalez RG. Quantification of microheterogeneity in glioblastoma multiforme with ex vivo high-resolution magic-angle spinning (HRMAS) proton magnetic resonance spectroscopy. Neuro-oncol 2000;2:87-95.

105 Cheng LL, Lean CL, Bogdanova A, et al. Enhanced resolution of proton NMR spectra of malignant lymph nodes using magic-angle spinning. Magn Reson Med 1996;36:653-8.

106 Cheng LL, Ma MJ, Becerra L, et al. Quantitative neuropathology by high resolution magic angle spinning proton magnetic resonance spectroscopy. Proc Natl Acad Sci U S A 1997;94:6408-13.

107 Calabi L, Alfieri G, Biondi L, De Miranda M, Paleari L, Ghelli S. Application of high-resolution magic-angle spinning NMR spectroscopy to define the cell uptake of MRI contrast agents. J Magn Reson 2002;156:222.

108 Carlotti C, Aussenac F, Dufourc EJ. Towards high-resolution 1H-NMR in biological membranes: magic angle spinning of bicelles. Biochim Biophys Acta 2002;1564:156-64.

109 Chen JH, Enloe BM, Fletcher CD, Cory DG, Singer S. Biochemical analysis using high-resolution magic angle spinning NMR spectroscopy distinguishes lipoma-like well-differentiated liposarcoma from normal fat. J Am Chem Soc 2001;123:9200-1.

110 Griffin JL, Mann CJ, Scott J, Shoulders CC, Nicholson JK. Choline containing metabolites during cell transfection: an insight into magnetic resonance spectroscopy detectable changes. FEBS Lett 2001;509:263-6.

111 Griffin JL, Walker L, Shore RF, Nicholson JK. High-resolution magic angle spinning 1H-NMR spectroscopy studies on the renal biochemistry in the bank vole (Clethrionomys glareolus) and the effects of arsenic (As3+) toxicity. Xenobiotica 2001;31:377-85.

112 Griffin JL, Walker LA, Shore RF, Nicholson JK. Metabolic profiling of chronic cadmium exposure in the rat. Chem Res Toxicol 2001;14:1428-34.

113 Griffin JL, Williams HJ, Sang E, Nicholson JK. Abnormal lipid profile of dystrophic cardiac tissue as demonstrated by one- and two-dimensional magic-angle spinning (1)H NMR spectroscopy. Magn Reson Med 2001;46:249-55.

114 Hu JZ, Rommereim DN, Wind RA. High-resolution 1H NMR spectroscopy in rat liver using magic angle turning at a 1 Hz spinning rate. Magn Reson Med 2002;47:829-36.

115 Morvan D, Demidem A, Papon J, De Latour M, Madelmont JC. Melanoma tumors acquire a new phospholipid metabolism phenotype under cystemustine as revealed by high-resolution magic angle spinning proton nuclear magnetic resonance spectroscopy of intact tumor samples. Cancer Res 2002;62:1890-7.

116 Schiller J, Naji L, Huster D, Kaufmann J, Arnold K. 1H and 13C HR-MAS NMR investigations on native and enzymatically digested bovine nasal cartilage. Magma 2001;13:19-27.

117 Sitter B, Sonnewald U, Spraul M, Fjosne HE, Gribbestad IS. High-resolution magic angle spinning MRS of breast cancer tissue. NMR Biomed 2002;15:327-37.

118 Tzika AA, Cheng LL, Goumnerova L, et al. Biochemical characterization of pediatric brain tumors by using in vivo and ex vivo magnetic resonance spectroscopy. J Neurosurg 2002;96:1023-31.

119 Waters NJ, Holmes E, Waterfield CJ, Farrant RD, Nicholson JK. NMR and pattern recognition studies on liver extracts and intact livers from rats treated with alpha-naphthylisothiocyanate. Biochem Pharmacol 2002;64:67-77.

120 Waters NJ, Holmes E, Williams A, Waterfield CJ, Farrant RD, Nicholson JK. NMR and pattern recognition studies on the time-related metabolic effects of alpha-naphthylisothiocyanate on liver, urine, and plasma in the rat: an integrative metabonomic approach. Chem Res Toxicol 2001;14:1401-12.

121 Wieruszeski JM, Montagne G, Chessari G, Rousselot-Pailley P, Lippens G. Rotor synchronization of radiofrequency and gradient pulses in high-resolution magic angle spinning NMR. J Magn Reson 2001;152:95-102.

122 Wind RA, Hu JZ, Rommereim DN. High-resolution (1)H NMR spectroscopy in organs and tissues using slow magic angle spinning. Magn Reson Med 2001;46:213-8.

123 Barton SJ, Howe FA, Tomlins AM, et al. Comparison of in vivo 1H MRS of human brain tumours with 1H HR-MAS spectroscopy of intact biopsy samples in vitro. Magma 1999;8:121-8.

124 Bollard ME, Garrod S, Holmes E, et al. High-resolution (1)H and (1)H-(13)C magic angle spinning NMR spectroscopy of rat liver. Magn Reson Med 2000;44:201-7.

125 Garrod S, Humpfer E, Spraul M, et al. High-resolution magic angle spinning 1H NMR spectroscopic studies on intact rat renal cortex and medulla. Magn Reson Med 1999;41:1108-18.

126 Garrod S, Humpher E, Connor SC, et al. High-resolution (1)H NMR and magic angle spinning NMR spectroscopic investigation of the biochemical effects of 2-bromoethanamine in intact renal and hepatic tissue. Magn Reson Med 2001;45:781-90.

127 Griffin JL, Troke J, Walker LA, Shore RF, Lindon JC, Nicholson JK. The biochemical profile of rat testicular tissue as measured by magic angle spinning 1H NMR spectroscopy. FEBS Lett 2000;486:225-9.

128 Griffin JL, Walker LA, Garrod S, Holmes E, Shore RF, Nicholson JK. NMR spectroscopy based metabonomic studies on the comparative biochemistry of the kidney and urine of the bank vole (Clethrionomys glareolus), wood mouse (Apodemus sylvaticus), white toothed shrew (Crocidura suaveolens) and the laboratory rat. Comp Biochem Physiol B Biochem Mol Biol 2000;127:357-67.

129 Griffin JL, Walker LA, Troke J, Osborn D, Shore RF, Nicholson JK. The initial pathogenesis of cadmium induced renal toxicity. FEBS Lett 2000;478:147-50.

130 Humpfer E, Spraul M, Nicholls AW, Nicholson JK, Lindon JC. Direct observation of resolved intracellular and extracellular water signals in intact human red blood cells using 1H MAS NMR spectroscopy. Magn Reson Med 1997;38:334-6.

131 Millis K, Weybright P, Campbell N, et al. Classification of human liposarcoma and lipoma using ex vivo proton NMR spectroscopy. Magn Reson Med 1999;41:257-67.

132 Millis KK, Maas WE, Cory DG, Singer S. Gradient, high-resolution, magic-angle spinning nuclear magnetic resonance spectroscopy of human adipocyte tissue. Magn Reson Med 1997;38:399-403.

133 Moka D, Vorreuther R, Schicha H, et al. Biochemical classification of kidney carcinoma biopsy samples using magic-angle-spinning 1H nuclear magnetic resonance spectroscopy. J Pharm Biomed Anal 1998;17:125-32.

134 Tate AR, Foxall PJ, Holmes E, et al. Distinction between normal and renal cell carcinoma kidney cortical biopsy samples using pattern recognition of (1)H magic angle spinning (MAS) NMR spectra. NMR Biomed 2000;13:64-71.

135 Waters NJ, Garrod S, Farrant RD, et al. High-resolution magic angle spinning (1)H NMR spectroscopy of intact liver and kidney: optimization of sample preparation procedures and biochemical stability of tissue during spectral acquisition. Anal Biochem 2000;282:16-23.

136 Weybright P, Millis K, Campbell N, Cory DG, Singer S. Gradient, high-resolution, magic angle spinning 1H nuclear magnetic resonance spectroscopy of intact cells. Magn Reson Med 1998;39:337-45.

137 Zektzer AS, Swanson MG, Jarso S, Nelson SJ, Vigneron DB, Kurhanewicz J. Improved signal to noise in high-resolution magic angle spinning total correlation spectroscopy studies of prostate tissues using rotor-synchronized adiabatic pulses. Magn Reson Med 2005;53:41-8.

138 Swanson MG, Vigneron DB, Tabatabai ZL, et al. Proton HR-MAS spectroscopy and quantitative pathologic analysis of MRI/3D-MRSI-targeted postsurgical prostate tissues. Magn Reson Med 2003;50:944-54.

139 Maxeiner A, Adkins CB, Zhang Y, et al. Retrospective Analysis of Prostate Cancer Recurrence Potential With Tissue Metabolomic Profiles. Prostate 2010;70:710-7.

140 Kaul D, Wu C, Adkins C, et al. Assessing prostate cancer growth with mRNA of spermine metabolic enzymes. Cancer Biol Ther 2010;9:[Epub ahead of print].

141 Smith R, Litwin M, Lu Y, Zetter B. Identification of an endogenous inhibitor of prostate carcinoma cell growth. Nature Med 1995;1:1040-5.

142 Mohan RR, Challa A, Gupta S, et al. Overexpression of ornithine decarboxylase in prostate cancer and prostatic fluid in humans. Clin Cancer Res 1999;5:143-7.

143 Higuchi C, Wang W. Comodulation of cellular polyamines and proliferation: biomarker application to colorectal mucosa. J Cell Biochem 1995;57:256-61.

144 Fernandez C, Sharrard R, Talbot M, Reed B, Monks N. Evaluation of the significance of polyamines and their oxidases in the aetiology of human cervical carcinoma. Br J Cancer 1995;72:1194-9.

145 Notarnicola M, Linsalata M, Caruso M, Cavallini A, Di Leo A. Low density lipoprotein receptors and polyamine levels in human colorectal adenocarcinoma. J Gastroenterol 1995;30:705-9.

146 Nishioka K, Melgarejo A, Lyon R, Mitchell M. Polyamines as biomarkers of cervical intraepithelial neoplasia. J Cell Biochem Suppl 1995;23:87-95.

147 Wang W, Liu L, Higuchi C. Mucosal polyamine measurements and colorectal cancer risk. J Cell Biochem 1996;63:252-7.

148 Ernestus R-I, Rohn G, Schroder R, et al. Polyamine metabolism in gliomas. J Neuro-Oncol 1996;29:167-74.

149 Chanda R, Ganguly A. Diamine-oxidase activity and tissue di- and poly-amine contents of human ovarian, cervical and endometrial carcinoma. Cancer Lett 1995;89:23-8.

150 Konety BR, Getzenberg RH. Novel therapies for advanced prostate cancer. Semin Urol Oncol 1997;15:33-42.

151 Lee S, Suh J, Chung B, Kim S. Polyamine profile in the urine of patiens with leukemia. Cancer Lett 1998;122:1-8.

152 Hiramatsu K, Sugimoto M, Kamei S, et al. Diagnostic and prognostic usefulness of N1,N8-diacetylspermidine and N1,N12-diacetylspermine in urine as novel markers of malignancy. J Cancer Res Clin Oncol 1997;123:539-45.

153 Cipolla B, Moulinoux J-P, Quemener V, et al. Erythrocyte polyamine levels in human prostatic carcinoma. J Urol 1990;144:1164-6.

154 Cipolla BG, Ziade J, Bansard JY, et al. Pretherapeutic erythrocyte polyamine spermine levels discriminate high risk relapsing patients with M1 prostate carcinoma. Cancer 1996;78:1055-65.

155 Liu X, Wang L, Lin Y, et al. Ornithine decarboxylase activity and its gene expression are increased in benign hyperplastic prostate. Prostate 2000;43:83-7.

156 Seiler N, Atanassov CL, Raul F. Polyamine metabolism as target for cancer chemoprevention (review). Int J Oncol 1998;13:993-1006.

157 Sharma RA, Manson MM, Gescher A, Steward WP. Colorectal cancer chemoprevention: biochemical targets and clinical development of promising agents. Eur J Cancer 2001;37:12-22.

158 Zakian K, Shukla-Dave A, Ackerstaff E, Hricak H, Koutcher J. 1H magnetic resonance spectroscopy of prostate cancer: biomarkers for tumor characterization. Cancer Biomark 2008;4:263-76.

159 Serkova N, Gamito E, Jones R, et al. The metabolites citrate, myo-inositol, and spermine are potential age-independent markers of prostate cancer in human expressed prostatic secretions. Eur Urol 2008;54:1198-9.

160 Cheng LL, Wu C, Smith MR, Gonzalez RG. Non-destructive quantitation of spermine in human prostate tissue samples using HRMAS 1H NMR spectroscopy at 9.4 T. FEBS Lett 2001;494:112-6.

161 Moinard C, Cynober L, de Bandt J. Polyamines: metabolism and implications in human diseases. Clin Nutr 2005;24:184-97.

162 Urdiales J, Medina M, Sánchez-Jiménez F. Polyamine metabolism revisited. Eur J Gastroenterol Hepatol 2001;13:1015-9.

163 Hillary R, Pegg A. Decarboxylases involved in polyamine biosynthesis and their inactivation by nitric oxide. Biochim Biophys Acta 2003;1647:161-6.

164 Tewari D, Qian Y, Thornton R, et al. Molecular cloning and sequencing of a human cDNA encoding ornithine decarboxylase antizyme". Biochim Biophys Acta 1995;1209:293–5.

165 Coffino P. Regulation of cellular polyamines by antizyme. Nat Rev Mol Cell Biol 2001;2:188-94.

166 Pegg AE. Recent advances in the biochemistry of polyamines in eukaryotes. Biochem J 1986;234:249-62.

167 Cotterman R, Jin V, Krig S, et al. N-Myc regulates a widespread euchromatic program in the human genome partially independent of its role as a classical transcription factor. Cancer Res 2008;68:9654-62.

168 Dominguez-Sola D, Ying CY, Grandori C, et al. Non-transcriptional control of DNA replication by c-Myc. Nature 2007;448:445-51.

169 Ullmanová V, Haškovec C. The Use of Housekeeping Genes (HKG) as an Internal Control for the Detection of Gene Expression by Quantitative Real-Time RT-PCR. Folia Biologica (Praha) 2003;49:211-6.

170 Zhu LJ, Altmann SW. mRNA and 18S-RNA coapplication-reverse transcription for quantitative gene expression analysis. Analytical Biochemistry 2005;345:102-9.

171 Yuan JS, Wang D, Stewart Jr. CN. Statistical methods for efficiency adjusted real-time PCR quantification. Biotechnol J 2008;3:112–23.

172 Heid C, Stevens J, Livak K, Williams P. Real time quantitative PCR. Genome Res 1996:986-94.

173 Yuan J, Reed A, Chen F, Stewart CN. Statistical analysis of real-time PCR data. BMC Bioinformatics 2006;7:85.

174 Schmittgen T, Zakrajsek B, Mills A, Gorn V, Singer M, Reed M. Quantitative reverse transcription-polymerase chain reaction to study mRNA decay: comparison of endpoint and real-time methods. Anal Biochem 2000:194-204.

175 Winer J, Jung CKS, Shackel I, Williams PM. Development and Validation of Real-Time Quantitative Reverse Transcriptase-Polymerase Chain Reaction for Monitoring Gene Expression in Cardiac Myocytesin Vitro. Analytical Biochemistry 1999;270:41-9.

176 Livak KJ, Schmittgen TD. Analysis of Relative Gene Expression Data Using Real-Time Quantitative PCR and the 2-[Delta][Delta]CT Method. Methods 2001;25:402-8.

177 Liu W, Saint D. Validation of a quantitative method for real time PCR kinetics. Biochem Biophys Res Commun 2002;294:347-53.

178 Swillens S, Dessars B, Housni H. Revisiting the sigmoidal curve fitting applied to quantitative real-time PCR data. Anal Biochem 2008;373:370-6.

179 Rutledge R. Sigmoidal curve-fitting redefines quantitative real-time PCR with the prospective of developing automated high-throughput applications. Nucleic Acids Res 2004;32:e178.

180 Rizzi F, Belloni L, Crafa P, et al. A novel gene signature for molecular diagnosis of human prostate cancer by RT-qPCR. Epub 2008;3:e3617.

181 Gardner T, Koch M. Prostate cancer therapy with high-intensity focused ultrasound. Clin Genitourin Cancer 2005;4:187-92.

182 Nag S, Beyer D, Friedland J, Grimm P, Nath R. American Brachytherapy Society (ABS) recommendations for transperineal permanent brachytherapy of prostate cancer. Int J Radiat Oncol Biol Phys 1999;44:789-99.

183 Perez C, Hanks G, Leibel S, Zietman A, Fuks Z, Lee W. Localized carcinoma of the prostate (stages T1B, T1C, T2, and T3). Review of management with external beam radiation therapy. Cancer 1993;72:3156-73.

184 Deger S, Taymoorian K, Boehmer D, et al. Thermoradiotherapy using interstitial self-regulating thermoseeds: an intermediate analysis of a phase II trial. Eur Urol 2004;45:574-9.

185 Bahn D, Lee F, Badalament R, Kumar A, Greski J, Chernick M. Targeted cryoablation of the prostate: 7-year outcomes in the primary treatment of prostate cancer. Urology 2002;60:3-11.

186 Robson M, Dawson N. How is androgen-dependent metastatic prostate cancer best treated? Hematol Oncol Clin North Am 1996;10:727-47.

187 Kupelian P, Elshaikh M, Reddy C, Zippe C, Klein E. Comparison of the efficacy of local therapies for localized prostate cancer in the prostate-specific antigen era: a large single-institution experience with radical prostatectomy and external-beam radiotherapy. Clin Oncol 2002;20:3376–85.

188 Schipper R, Deli G, Deloyer P, Lange W, Schalken J, Verhofstad A. Antitumor activity of the polyamine analog N(1), N(11)-diethylnorspermine against human prostate carcinoma cells. Prostate 2000;44:313-21.

189 Dunzendorfer U, Knöner M. Therapy with inhibitors of polyamine biosynthesis in refractory prostatic carcinoma. An experimental and clinical study. Onkologie 1985;8.

190 Zhang Y, Liu X, Zhang B, Hu H, Gong L. Antitumor effect of antisense ODC adenovirus on human prostate cancer cells. Prostate Cancer Prostatic Dis 2005;8.

191 Noh D-Y, Ahn S-J, Lee R-A, et al. Overexpression of phospholipase D1 in human breast cancer tissues. Cancer Letters 2000;161:207-14.

Selbstständigkeitserklärung

Hiermit erkläre ich, Florian Sturm, an Eides Statt, dass die vorgelegte Arbeit mit dem Thema *Linking Prostate Cancer Recurrence to the Spermine Pathway: A Retrospective Study using High Resolution Magic Angle Spinning 1H Magnetic Resonance Spectroscopy at 14T and Quantitative Polymerase Chain Reaction* von mir selbst und ohne die unzulässige Hilfe Dritter verfasst wurde, auch in Teilen keine Kopie Arbeiten anderer darstellt und die benutzten Hilfsmittel sowie die verwendete Literatur vollständig angegeben sind.

_____ _____

Ort, Datum ***Unterschrift***

[Mein Lebenslauf wird aus datenschutzrechtlichen Gründen
in der elektronischen Version meiner Arbeit nicht veröffentlicht.]

[Mein Lebenslauf wird aus datenschutzrechtlichen Gründen
in der elektronischen Version meiner Arbeit nicht veröffentlicht.]